Rock Magnetism
and
Paleogeophysics

Volume 19

December 1992

Preface

This volume is the annual progress report of the Rock Magnetism and Paleogeophysics Research Group in Japan for the year of 1992. We have published annual reports with a title Annual Progress Report of the Rock Magnetism (Paleogeophysics) Research Group in Japan in 1963, 1964, 1965, and 1967. Since 1973, the title changed to Rock Magnetism and Paleogeophysics and the reports were published annually (except 1976).

This volume contains a collection of summaries, extended abstracts or brief notes of research works carried out in our group this year. Many reports contain materials which may undergo a significant change or may be revised as the research activity continues. In this respect, readers are warned to regard them as tentative and are also requested to refer from a complete paper if published as a final results. (Names of journal appear at the end of individual articles if they are in press, submitted, or in preparation for submission to some scientific journals.

The editor of Rock Magnetism and Paleogeophysics has been Professor Masaru Kono of Tokyo Institute of Technology since 1973. However, as stated in the preface of volume 16, 1989, he decided to retire from the editorial charge. After some debate about the continuation of the annual report in our group, we decided to continue the publication of this annual report for more several years. During this extension period, M. Torii of Kyoto University is the editor of this report for even-number years and Y. Hamano of University of Tokyo for odd-number years.

Kyoto
December 1992

Masayuki Torii
Editor in 1992

Rock Magnetism and Paleogeophysics
Research Group in Japan

Rock Magnetism and Paleogeophysics, Volume 19
Table of Contents

ROCK MAGNETIC PROPERTIES OF BASALTIC ROCKS FORMED AT SEDIMENT-COVERED SPREADING CENTERS

Koji FUKUMA

Department of Geology and Mineralogy, Kyoto University, Kyoto 606-01, Japan

Here we present various rock magnetic properties on drilled basaltic rocks collected from two typical basins formed at sediment-covered spreading centers: the Yamato Basin of the Japan Sea and Middle Valley of the northern Juan de Fuca Ridge. In the past, thick sediment cover and/or high-temperature environments have precluded the drilling into ancient or present sediment-covered spreading centers. Therefore we could not discuss the causal relationship between sediment cover and the absence of lineated or positive magnetic anomalies based on the rock magnetic data themselves. However, recently Ocean Drilling Program (ODP) Legs 127 and 128 could penetrated the basaltic rocks underlying about 500 m thick sediments in the Yamato Basin of the Japan Sea, which is not accompanying lineated magnetic anomalies. Rock magnetic properties of these basaltic rocks will give a clue to clarify the reason for the absence of magnetic lineations in this marginal basin. ODP Leg 135 in Middle Valley of the northern Juan de Fuca Ridge provided the basaltic sill samples below about 500 m thick sediment sequence. Middle Valley is an ideal field to investigate the causal relationship between thick sediment cover and the overlying subdued marine magnetic anomaly at present spreading centers.

Rock magnetic properties of basaltic rocks formed beneath sedimented rifts are obtained from the drilled cores at Ocean Drilling Program (ODP) Site 794 (40.19°N, 138.23°E) in the Yamato Basin of the Japan Sea (Ingle, Suyehiro, von Breymann, et al., 1990) and ODP Site 857 (48.44°N, 128.71°W) in Middle Valley of the northern Juan de Fuca Ridge (Davis, Mottl, Fisher, et al., 1992).

ODP drilling results demonstrated that the uppermost crust is composed of basaltic intrusive rocks intercalated with sediment at both sites, although the tectonic settings are distinctively different from each other. The Yamato Basin is a remnant back-arc basin formed at 18-21 Ma (Kaneoka et al., 1992). The recovered core at Site 794 consists of about 200 m thick basaltic rocks which is intervened by sediment and overlaid by about 500 m sequence of sediment. These basaltic rocks are divided into nine lithologic units composed of either dolerite sills or doleritic basalt flows. These rocks were subject to extensive but moderate hydrothermal alteration at about 200°C during or immediately after emplacement (Allan and Gorton, 1992; Proust et al., 1992). Middle Valley is an active rift valley which is filled with the hemipelagic and turbidite sediment supplied from the nearby continental margin. Site 857 is located in a hydrothermal reservoir zone well within Middle Valley. Beneath about 500 m thick sediment sequence the first series of basaltic sills is encountered, and these sills range from about 1 to 25 m in thickness and are intercalated in approximately equal proportion with sediment. This sequence of sills and sediment persists to 936 m below the seafloor. These sills have suffered intense hydrothermal alteration characterized by the presence of epidote, chlorite and pyrite as secondary minerals. The in situ temperature is estimated to be about 300 °C (Davis and Villinger, 1992). In both cores none of extrusive pillow basalt was not found, which is typical for the uppermost part of oceanic crust.

Magnetic anomalies over the Yamato Basin show no clear lineated pattern over the whole basin and are characterized by low amplitude (<200 nT peak to peak) (Isezaki, 1986). Some features of the magnetic anomalies are associated with the seamounts trending approximately NE-SE along the axis of the basin (Sayanagi et al., 1987). Over Middle Valley, positive magnetic anomaly is expected to be observed because the area around Middle Valley has been formed during the present Brunhes normal polarity epoch. However the observed magnetic anomaly over Middle Valley locally exhibits more or less negative values along the valley axis.

The magnetic properties of the basaltic rocks at Site 794 in the Yamato Basin are characterized by lower magnetic stability and comparable concentration of magnetic material (Figure 1), compared to typical oceanic basalts represented by the basalt section of ODP Hole 504B (Pariso and Johnson, 1991). The dominant magnetic carriers are variably oxidized titanomaghemite (Curie temperature: 250-450 °C) which is an alteration product of primary titanomagnetite as often observed in oceanic basalts (Ozima and Ozima, 1971). Our electron microscope observation confirmed ubiquitous large (> several tens of μm) titanomaghemite grains with well developed shrinkage cracks (Petersen and Vali, 1987). No exsolution or granulation is observed under a microscope. Hysteresis properties show high saturation magnetization values (Js), low ratios of saturation remanence to saturation magnetization (Jrs/Js). And the remanence properties are as follows; (a) Natural remanent magnetization (NRM) intensities of these basaltic rocks are significantly lower than oceanic basalts particularly for dolerite sills. (b) The intensity of magnetization induced in the present geomagnetic field is comparable to that of NRM. (That is, the average of Koenigsberger ratios is nearly unity.) (c) The viscous remanent magnetization probably contributes the in situ remanent magnetization to a great extent. In addition, stable inclinations determined through alternating field demagnetization show the mixed polarity within the drilled hard rock sequence at Site 794. These magnetic properties suggest that the basaltic rocks recovered from Site 794 cannot be counted as a source of lineated magnetic anomaly due to its low remanence intensity and stability.

On the other hand, the basaltic sills recovered from Site 857 in Middle Valley have very low content of magnetic material and comparable stability relative to those of 504B (Figure 2). And the dolerite sills at Site 857 are quite different from oceanic basalts also in magnetic mineralogy. By thermomagnetic analyses and other magnetic methods, nearly pure magnetite was shown to be dominant magnetic carriers of these rocks. Primary Fe-Ti oxides are thoroughly granulated into magnetite and Ti-bearing phases as described by Ade-Hall et al. (1971). Very low Js and susceptibility values, which are more than one order smaller than oceanic basalts, suggesting that the content of magnetic material is much less than oceanic basalts. Hence NRM intensity and Koenigsberger ratio are greatly reduced compared to oceanic basalts. Meanwhile, the parameters related to magnetic stability such as Jrs/Js is not quite deviated from those of Hole 504B. Alternating field demagnetization enabled us to obtain stable inclination values consistent to the expected value (66°) from the geocentric axial dipole from the upper portion. Since drilling induced remanence (Audunsson and Levi, 1989) severely masks stable remanence, we could not determine the stable components of magnetization in the lower portion. But the in situ magnetization of basaltic sills at Site 857 appears to be consistently positive throughout the drilled section, because without exception the higher coercivity components of magnetization
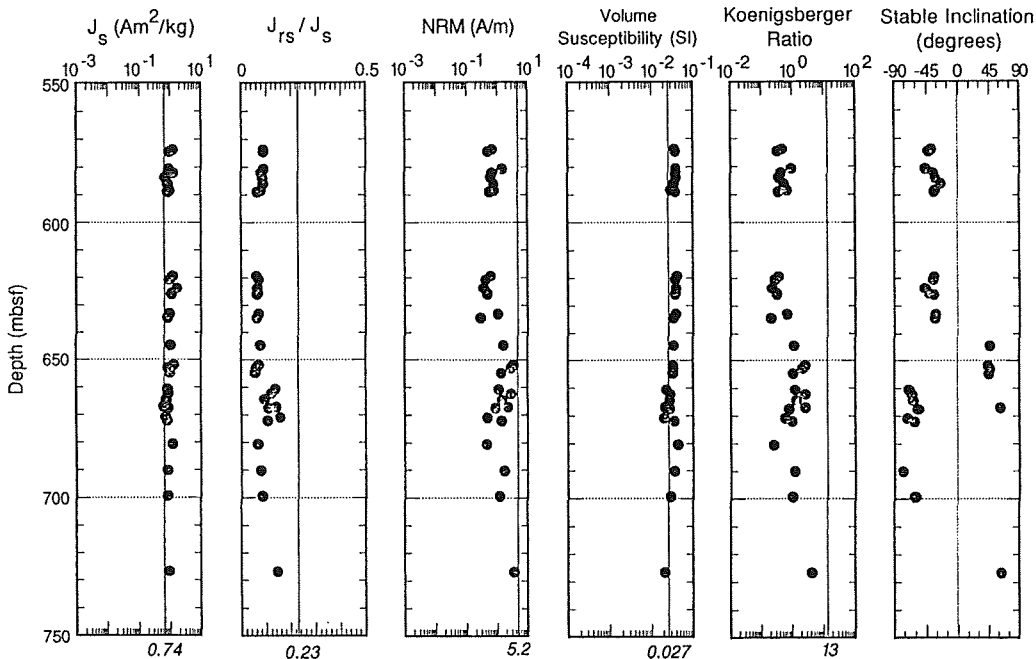
Figure 1. Profiles of magnetic properties from ODP Site 794 in the Yamato Basin of the Japan Sea. Depth is represented by meters below seafloor (mbsf). A vertical line in each graph represents the average value of the basalt section of ODP/DSDP Hole 504B (Pariso and Johnson, 1991).
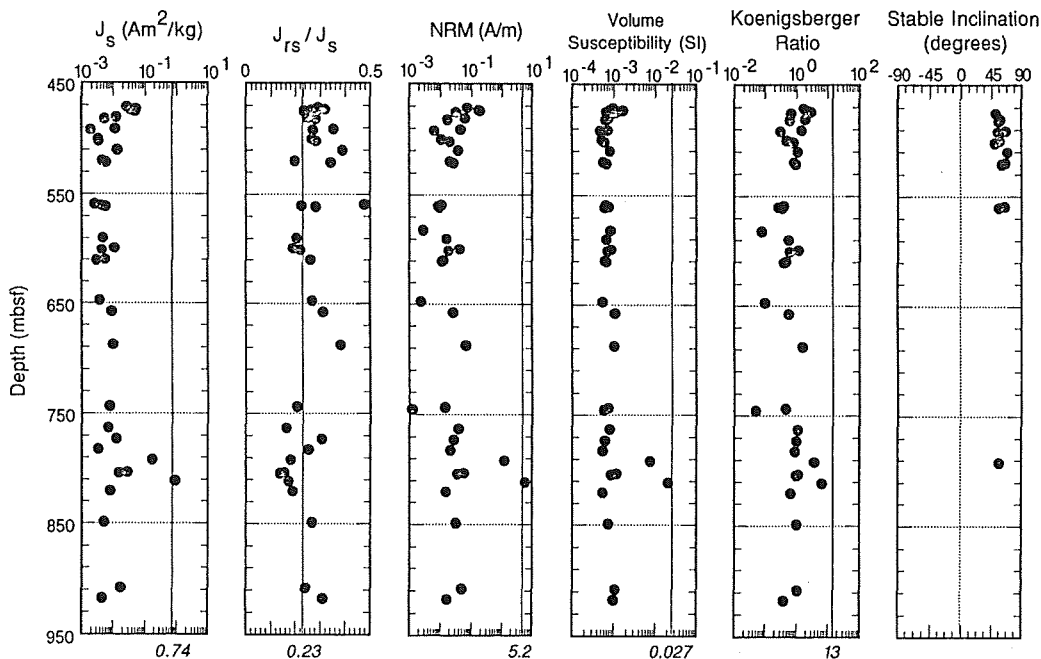

Figure 2. Profiles of magnetic properties from ODP Site 857 in Middle Valley of the northern Juan de Fuca Ridge. Depth is represented by meters below seafloor (mbsf). A vertical line in each graph represents the average value of the basalt section of ODP/DSDP Hole 504B (Pariso and Johnson, 1991).

3

show positive polarity during alternating field demagnetization. Due to very low NRM intensity, we can eliminate the possibility that the basaltic sills at Site 857 can significantly contribute to the magnetic anomaly. Note that a portion around 800 meter below seafloor (mbsf) exhibits the high concentration and NRM intensity associated with low stability.

We will discuss factors dominating rock magnetic properties obtained from these sites in the following view point; The magnetic properties are a function of both the primary igneous history and the subsequent alteration history of rocks. Hence we should take into consideration both the effect of grain size of original magnetic minerals and alteration degrees in relation to magnetic properties.

Low NRM intensity and low stability for Site 794 mainly appears to be attributed to the large grain size of magnetic minerals formed during intrusion. Although it is usually observed that fine-grained titanomaghemite is more oxidized than coarse-grained one in the same condition (Johnson and Hall, 1978; Nishitani and Kono, 1982), we could not find gross difference in Tc (positively correlated to the degree of maghemitization (Readman and O'Reilly, 1972; Keefer and Shive, 1981; Ozdemir and O'Reilly, 1981; Nishitani and Kono, 1983) between the basaltic rocks of Site 794 and Hole 504B in spite of their different lithologic types. Note the observed large (> several tens of μm) titanomaghemite, which is in multidomain size range (Ozdemir and Banerjee, 1981). Although it is difficult to separate the effect of grain size and maghemitization on magnetic properties, grain size effect appears to predominate the different magnetic parameters between 794 and 504B such as Jrs/Js, NRM intensity and Koenigsberger ratio. Some submarine doleritic basalts are reported to have low NRM intensity and large viscous component of remanence whatever the degree of maghemitization from cores drilled at DSDP Hole 417A and 417D (Smith, 1987). Moskowitz and Banerjee (1981) reported that most of magnetic properties are distinctively different between fine-grained pillow basalts and coarse-grained massive flows from 417D. Although they refer to the difficulty of separating the effect of grain size and maghemitization on magnetic properties, they suggests that grain size effect predominate. Taking account of these results, we conclude that the magnetic properties of the basaltic rocks of Site 794 are due to the coarse-grained magnetic minerals which is originally formed by intrusion of magma into soft sediment cover. Subsequent moderate hydrothermal alteration only made minor effect on magnetic properties.

Magnetic properties of Site 857 are well influenced by intense hydrothermal alteration associated with formation of nearly pure magnetite. Very low Js and susceptibility values indicate that the basaltic sills of Site 857 contain much less magnetic material than oceanic basalts. And fairly high magnetic stability, estimated from large Jrs/Js values, suggests small effective magnetic grain size. We suppose that intense hydrothermal alteration of magnetic minerals, including extensive iron leaching from the original Fe-Ti oxides, results in the reduction of both content of magnetic material and effective magnetic grain size. Optical evidences support this mechanism for Site 857 sills. Under the reflected-light microscope, Fe-Ti oxide phenocrysts appear to be almost ghost, suggesting "granulation" as described by Ade-Hall et al. (1971). In this process, a titanium-bearing phase is formed from the primary homogeneous titanomagnetite or deuterically oxidized titanomagnetite, and iron either remains in the magnetite host or is leached from the spinel lattice. Similar processes are previously reported from the transition zone in 504B (Pariso and Johnson, 1991) and in the Troodos ophiolite (Hall et al.,

1987) between basalt section and sheeted dike section. We infer that the presence of magnetite and extremely low NRM intensity in Site 857 sills is attributed to intense hydrothermal alteration beneath thick sediment blanket (Davis and Lister, 1977). This explanation is conversely applicable to the less altered portion around 800 mbsf with high NRM intensity and Js.

Based on various magnetic properties and observation of magnetic minerals, we can show two extreme cases resulted in the reduction of remanence intensity and Koenigsberger ratio; One is associated with the large grain size due to the initial slow cooling in the Yamato Basin and the other is with the low concentration of magnetic material due to intense hydrothermal alteration in Middle Valley. For the former case sediment cover leads to forming intrusive basaltic rocks, and for the latter case, in addition to the formation of intrusives, relatively impermeable sediment cover limits the recharge of hydrothermal fluids and thermally insulates the underlying crust (Davis and Villinger, 1992). Extensive but moderate hydrothermal alteration characterized by the presence of titanomaghemite do not appear to result in a significant reduction of magnetic material as seen for the Yamato Basin. Intense hydrothermal alteration leading to the formation of magnetite is required to explain the reduced remanence intensity in view of the reduced content of magnetic materials as for Middle Valley. It is sure that the in situ high temperature of about 300°C in Middle Valley somewhat contributes to reducing the remanent magnetization in situ, but the amount of the reduction reaches only 20% of the room temperature value at most (Pullaiah et al., 1975).

Finally we will discuss the implication for the absence of lineated or positive magnetic anomalies over the Yamato Basin or Middle Valley. For Middle Valley, intense hydrothermal alteration caused by sediment cover appears to sufficiently explain the absence of positive magnetic anomaly, because the deeper crust is unlikely to contribute to magnetic anomaly at active spreading centers significantly. Observed local negative magnetic anomaly along the axis of Middle Valley is probably due to the edge effect due to the positively magnetized crustal block at south. For the Yamato Basin we note the mixed polarity of stable magnetization within a single hole at Site 794. These results suggests the multiple emplacement of each lithologic unit over several geomagnetic polarity epochs, which is supported by the distinctive geochemical data between the upper and lower units (Ingle, Suyehiro, von Breymann, et al., 1990; Tamaki, Pisciotto, Allan, et al., 1990; Allan and Gorton, 1992; Thy, 1992) and the significantly younger age of the basal sediment above the uppermost unit (Tamaki, Pisciotto, Allan, et al., 1990) relative to the ^{40}Ar-^{39}Ar age from the lower units (Kaneoka et al., 1992). In addition to the effect of sediment cover, later volcanism may have obscured the magnetic anomaly patterns in the Yamato Basin as proposed by Kono (1986).

References

Ade-Hall, J. M., Palmer, H. C. and Hubbard, T. P. (1971) *Geophys. J. R. astr. Soc.*, 24, 137-174.

Allan, J. F. and Gorton, M. G. (1992) *Proc. ODP, Sci. Results*, 127/128, Pt.2, 905-929.

Davis, E. E. and Lister, C. R. B. (1977) *Bull. Geol. Soc. Am.*, 88, 346-363.

Davis, E. E., Mottle, M. J. and Fisher, A. T., et al. (1992) *Proc. ODP, Init. Repts.*, 139.

Davis, E. E. and Villinger, H. (1992) *Proc. ODP, Init. Repts.*, 139, 9-41.

Hall, J. M., Fisher, B. E., Walls, C. C., Hall, S. L., Johnson, H. P., Bakor, A. R., Agrawal, V., Persaud, M. and Sumatang, R. M. (1987) *Nature,* 326, 780-782.

Ingle, J. C., Suyehiro, K. and von Breymann, M. T., et al. (1990) *Proc. ODP, Init. Repts.*, 128.

Isezaki, N. (1986) *J. Geomag. Geoelectr.,* 38, 403-410.

Johnson, H. P. and Hall, J. M. (1978) *Geophys. J. R. astr. Soc.,* 52, 45-64.

Kaneoka, I., Takigami, Y., Takaoka, N., Yamashita, S. and Tamaki, K. (1992) *Proc. ODP, Sci. Results,* 127/128, Pt. 2, 819-836.

Keefer, C. M. and Shive, P. N. (1981) *J. Geophys. Res.,* 86, 987-998.

Kono, M. (1986) *J. Geomag. Geoelectr.,* 38, 411-426.

Moskowitz, B. M. and Banerjee, S. K. (1981) *J. Geophys. Res.,* 86, 11869-11882.

Nishitani, T. and Kono, M. (1982) *J. Geophys.,* 50, 137-142.

Nishitani, T. and Kono, M. (1983) *Geophys. J. R. astr. Soc.,* 74, 585-600.

Ozdemir, O. and Banerjee, S. K. (1981) *J. Geophys. Res.,* 86, 11864-11868.

Ozdemir, O. and O'Reilly, W. (1981) *J. Geophys.,* 49, 93-100.

Ozima, M. and Ozima, M. (1971) *J. Geophys. Res.,* 76, 2051-2056.

Pariso, J. E. and Johnson, H. P. (1991) *J. Geophys. Res.,* 96, 11703-11722.

Petersen, N. and Vali, H. (1987) *Phys. Earth Planet. Int.,* 46, 197-205.

Proust, D., Meunier, A., Fouillac, A. M., Dudoignon, P., Sturz, A., Charvet, J. and Scott, S. D. (1992) *Proc. ODP, Sci. Results,* 127/128, Pt. 2, 883-889.

Pullaiah, G., Irving, E., Buchan, K. L. and Dunlop, D. J. (1975) *Earth Planet. Sci. Lett.,* 28, 133-143.

Readman, P. W. and O'Reilly, W. (1972) *J. Geomag. Geoelectr.,* 24, 69-90.

Sayanagi, K., Isezaki, N. and Kitahara, Y. (1987) *Bull. Earthq. Res. Inst.,* 62, 391-415.

Smith, B. M. (1987) *Phys. Earth Planet. Inter.,* 46, 206-226.

Tamaki, K., Pisciotto, K. and Allan, J., et al. (1990) *Proc. ODP, Init. Repts.*, 127.

Thy, P., (1992). *Proc. ODP, Sci. Results,* 127/128, Pt. 2, 849-859.

ROCK MAGNETISM AND MAGNETIC ANOMALIES OF THE MIYAMORI ULTRAMAFIC COMPLEX, JAPAN

Shigeo OKUMA, Toshiyuki TOSHA and Hiroshi KANAYA

Geological Survey of Japan, 1-1-3 Higashi, Tsukuba, Ibaraki, 305 Japan

1. Introduction

Rock magnetic measurements are not only indispensable for paleomagnetic study, but also for magnetic exploration. However, the rock magnetic measurements for magnetic exploration has not been intensively conducted in Japan so far. Most of them are limited to only the measurements of magnetic susceptibility and often lack the measurements of remanent magnetization.

Therefore, we had started studies on the rock magnetism and its application for magnetic exploration in the Kitakami Mountains, northeast Japan. Okuma and Kanaya (1990) have already presented a report on the rock magnetism and magnetic anomalies of the Kitakami granitic rocks (KGR). They revealed that the KGR show relatively high magnetic susceptibility (> 1.0 $\times 10^{-2}$ SI) compared to ordinary granitic rocks and low Qn ratio (0.1 ~ 0.3). In additional results of paleomagnetism with northwestern declination and downward inclination of the KGR (e.g. Kawai et al., 1971), magnetic anomalies of the KGR are caused mainly by magnetic susceptibility of the rocks. Actually, most magnetic anomalies are distributed over the exposures of the KGR. Furthermore, reduction to the pole anomalies, on assumption that the KGR are magnetized in the direction of the present Earth's magnetic field, are distributed right over them. Some of these magnetic anomalies are distributed along the coast lines and further extends offshore in the Pacific Ocean. Drilling at an offshore extension of those anomalies has reached a Cretaceous granitic rocks at 1,840 m below sea level (Japanese Association of Natural Gas, 1986).

On the other hand, magnetic anomalies of the Miyamori ultramafic complex (MUC) (Fig.1 and 2) with amplitude larger than 1,000 nT are predominant, compared to those of the KGR with mean amplitude of few hundreds nT in the Kitakami Mountains (Fig.3). Hence, we began a study on the rock magnetism and magnetic anomalies of the complex. This paper describes a preliminary result of the study.

2. Geology

The MUC has a length of approximately 40 km and a maximum width of 7 km (Ozawa, 1984). The eastern part of the complex is bounded by the Hizume-Kesennuma Fault, while western part was intruded by an early Cretaceous granodiorite whose contact metamorphism affects more than half of the complex (Seki, 1951a, b). The K-Ar ages for gabbroic rocks from the MUC range from 421 to 484 Ma and most of them correspond to Ordovician (445 ~ 484 Ma) (Ozawa et al., 1988). Ozawa (1984) argued that the MUC is a thin thrust sheet, which comprises a tectonic member, a cumulative member and gabbroic rocks. He defined that the tectonite member is composed dominantly of hornblende-bearing harzburgite, dunite, and hornblende peridotite, while that
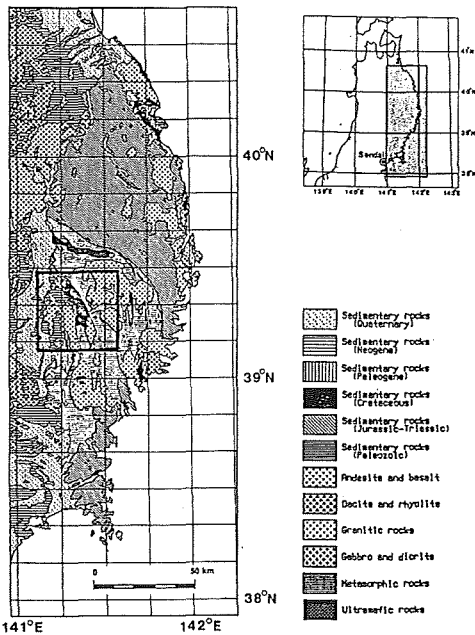
Fig.1 Location map of study area.
Enclosed part with solid lines on a geologic map (after Yamada *et al.*, 1982) corresponds to study area.
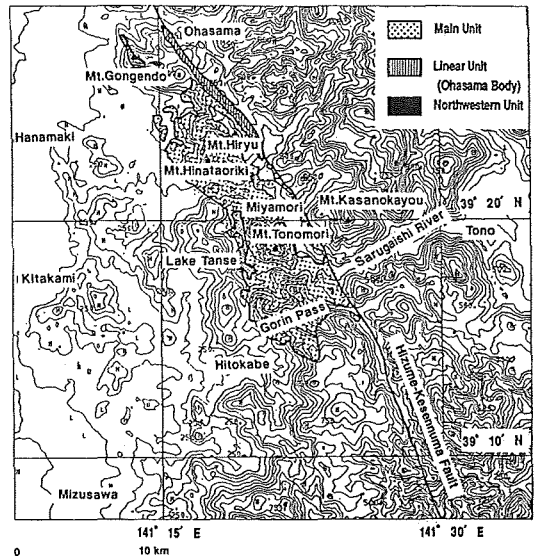
Fig.2 Distribution map of the Miyamori ultramafic complex (after OZAWA, 1984).
Contour interval of topography is 50 m.
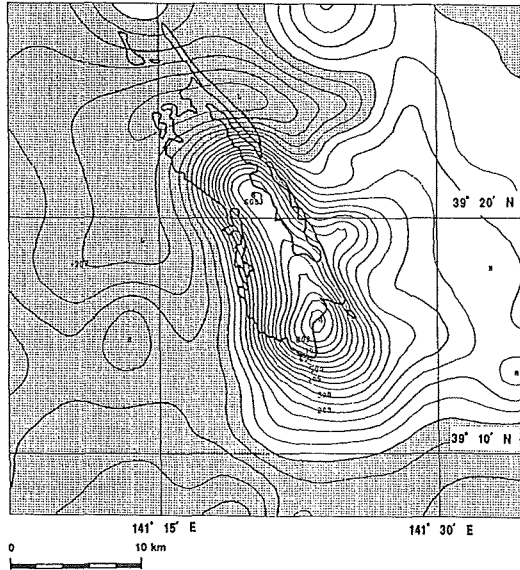
Fig.3 Magnetic anomalies in and around the Miyamori ultramafic complex at an elevation of 2,440 m (8,000 feet) above sea level (after NEDO, 1982).
Contour interval is 50 nT. Dotted areas show negative magnetic anomalies. Thick solid lines indicate the Miyamori ultramafic complex.
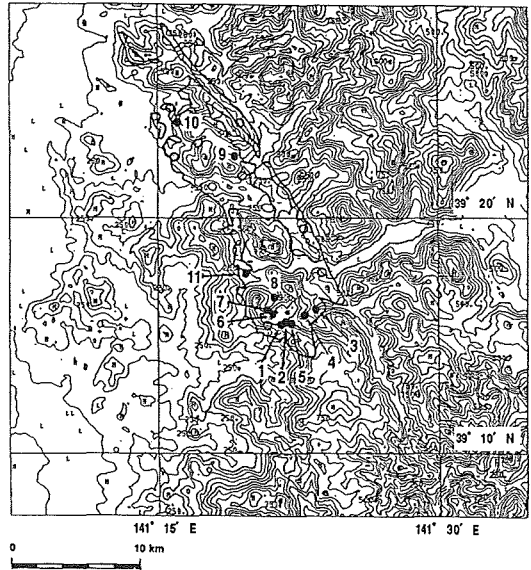
Fig.4 Sampling sites of rock samples for rock magnetic measurements.

●: Sampling sites, ○:Sites from which rock samples of magnetic susceptibility more than 1 X 10^{-2} (SI) were collected. Numbers (1 - 11) on the map show sampling sites.

the cumulative member consists mainly of hornblende-bearing dunite, wehrlite, and olivine clinopyroxenite. He suggested that the MUC is a fragment of the upper mantle formed under H_2O-rich conditions in an island arc, because of the presence of hornblende in any type of mafic and ultramafic rocks as a major constituent mineral. He also suggested that the MUC was a portion of the Hayachine complex and transported to the south along the Hizume-Kesennuma Fault before early Cretaceous, based on the similarities of peridotites between the two complexes.

3. Rock magnetism

We collected twenty-seven rock samples from eleven outcrops by hand (Fig.4). Most of the samples are serpentinites. Major minerals in the samples were described by Dr. Katada, emeritus professor of Iwate Univ. (Katada, personal communication). According to the classification of Ozawa (1984), the collected samples are composed of tectonite members, cumulative members and gabbroic rocks. Each sample comprises three cylindrical specimens with diameter and thickness of one inch. Magnetic susceptibility and natural remanent magnetization of the specimens were measured using a Model 3101 magnetometer (BISON Ltd) and SMM-85 magnetometer (Natsuhara Giken Co.), respectively. A mean value of rock magnetism for each sample was calculated from the values of its three specimens. The measurements indicated that twenty-four samples were valuable for a further discussion among the twenty-seven samples. We did not perform any magnetic cleaning on the specimens, because the main subject of this study is to analyze magnetic anomalies in this region.

Table 1 shows the result of the measurements. Fig.5 indicates histograms of magnetic susceptibility (κ) and natural remanent magnetization (Jn) of the samples. Fig.6 shows a histogram of Königsberger ratio (Qn ratio) and a graph of Jn versus κ of the samples. The direction of Jn for each sample is plotted in an equal area net (Fig.7). Fig.7 reveals that all inclinations of the samples are downward and most of declinations are in the fourth quadrant. Qn ratio ranges from 0.32 to 4.33 and the mean value of them is 1.90. This result shows that we have to take account of remanent magnetization in addition to induced magnetization when we analyze magnetic anomalies in this region. The mean magnetic susceptibility of the samples is 8.16×10^{-2} SI. The mean intensity, inclination and declination of natural remanent magnetization of the samples are 6.15 (A/m), 52.4 ° N and 54.3 ° W, respectively. On the other hand, the intensity, inclination and declination of the present Earth's magnetic field in study area are 47,500 nT, 53.0 ° N and 7.5 ° W, respectively.

4. Analysis of magnetic anomalies

Forward modeling was conducted to analyze magnetic anomalies of MUC. Synthetic magnetic anomalies were calculated from one or two horizontal polygon models in layers by the method of Talwani (1965). Observed total force magnetic anomalies and synthetic anomalies were compared each other (Fig.8). The shape of the layer was determined by the exposure of the MUC in the geologic map (OZAWA, 1984) and the distribution of the rock samples with strong intensity.

Table 1 Result of rock magnetic measurements of the rock samples.

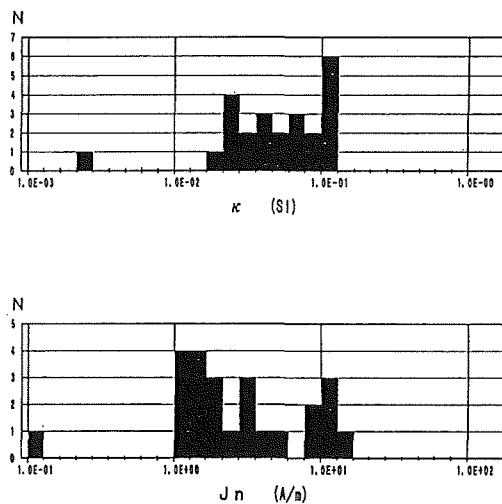| Sample Name	J_0 (×10^n) (A/m)	n	κ (×10^n) (SI)	n	Q_0	Declination (°)	Inclination (°)
1-1	2.54	0	4.00	-2	1.68	-24.8	62.6
1-2	7.07	0	6.03	-2	3.10	-17.1	61.3
2-1	1.00	1	9.32	-2	2.84	-22.4	46.6
2-2	3.85	0	7.54	-2	1.35	-46.8	47.3
3-1	6.89	0	4.66	-2	3.91	-26.8	51.6
3-2	4.78	0	8.14	-2	1.55	-44.0	58.6
4-1	9.83	0	6.86	-2	3.79	-41.7	53.6
4-2	1.40	1	8.57	-2	4.33	-74.2	63.9
5-1*	1.99	-4	3.14	-4	0.02		
5-2*	2.44	-4	3.14	-4	0.02		
6-1	1.19	1	1.81	-1	1.74	-55.6	62.0
6-2	1.73	1	1.20	-1	3.80	-38.9	52.7
6-3	1.68	1	1.68	-1	3.54	-32.0	67.1
7-1*	2.12	-2	5.15	-4	1.09		
7-2	1.64	-1	4.81	-3	0.90	-39.6	50.7
8-2	2.93	0	8.92	-2	0.87	-49.5	54.2
8-3	5.05	0	1.02	-1	1.31	-58.3	55.5
9-1	2.92	0	4.36	-2	1.77	-41.8	49.4
9-2	3.38	0	5.58	-2	1.60	-79.6	69.4
9-3	5.55	0	6.85	-2	2.14	-45.2	51.4
10-1	1.29	0	4.90	-2	0.70	-57.3	53.3
10-2	1.61	0	5.22	-2	0.82	-58.3	58.3
10-3	1.72	0	4.99	-2	0.91	-81.8	59.9
11-1	2.25	0	7.21	-2	0.83	-78.8	30.6
11-2	1.12	0	9.31	-2	0.32	-70.2	21.8
11-3	3.76	0	1.14	-1	0.87	-77.3	16.4
11-4	5.09	0	1.43	-1	0.94	-91.3	7.2

(5-1)*, (5-2)*, (7-1)*: Excluded for a further discussion.

Fig.5 Histograms of magnetic susceptibility (upper) and natural remanent magnetization (lower) of the rock samples, respectively.
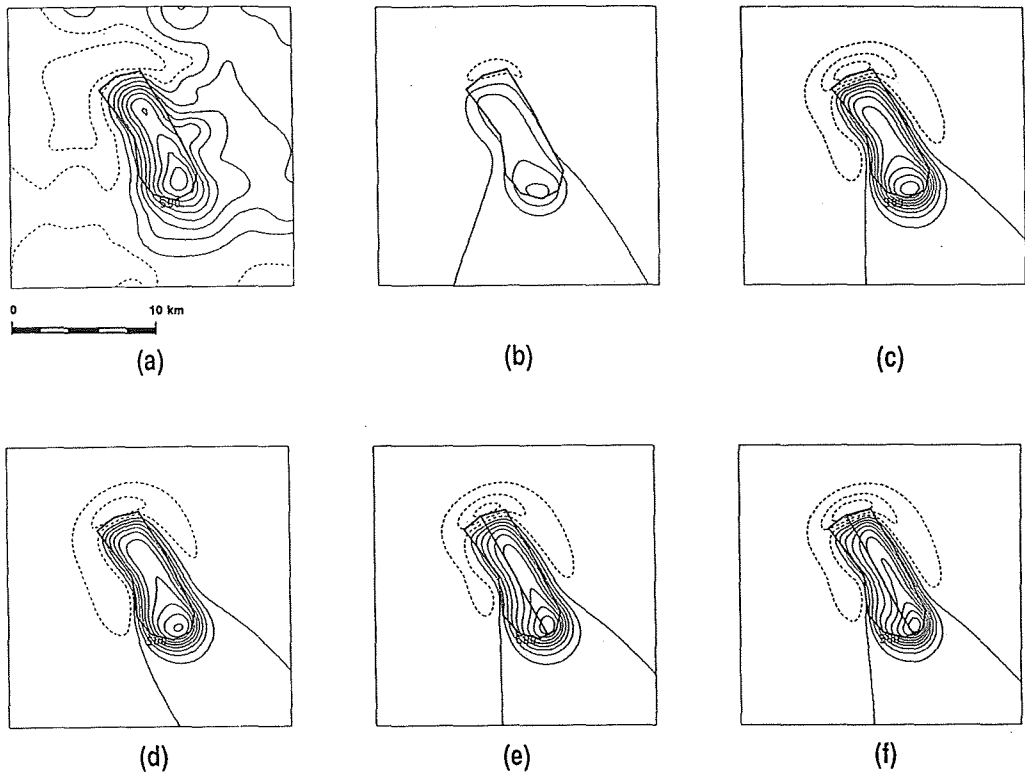

Fig.6 Histogram of Qn ratio (upper) and natural remanent magnetization versus magnetic susceptibility of the rock samples (lower), respectively.
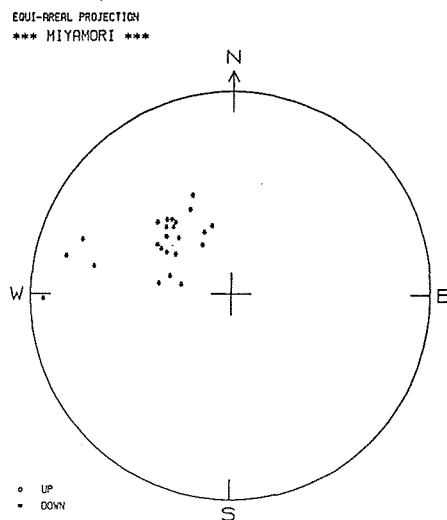
Fig.7 Equal area projection of natural remanent magnetization of the rock samples.

Fig.8

(a) Observed total force aeromagnetic anomalies in and around the Miyamori ultramafic complex at an elevation of 2,440 m above sea level (after NEDO, 1982).
Contour interval is 100 nT. A simplified horizontal polygon model corresponds to the complex.

(b) Synthetic magnetic anomalies caused by a horizontal polygon model. The magnetic susceptibility of the model is 8.16×10^{-2} (SI).
The intensity, inclination and declination of the Earth's magnetic field are 47,500 nT, 53.0 °N and 7.5 ° W, respectively. The top height of the model is 340 m above sea level. The thickness of the model is 1,300 m.

(c) Synthetic magnetic anomalies caused by a horizontal polygon model. In addition to (b), the magnetization intensity is 6.15 (A/m) with the inclination of 52.4 ° N and declination of 54.3 ° W.

(d) Synthetic magnetic anomalies caused by a horizontal polygon model. In addition to (b), the magnetization intensity is 6.15 (A/m) with the inclination of 52.4 ° N and declination of 91.3 ° W.

(e) Synthetic magnetic anomalies caused by two horizontal polygon models in layers. The magnetic susceptibility of the both upper large model and lower small model is 8.16×10^{-2} (SI).
The magnetization intensity is 6.15 (A/m) with the inclination of 52.4 ° N and declination of 54.3 ° W. The thicknesses of the both models are equally 750 m.

(f) Synthetic magnetic anomalies caused by two horizontal polygon models in layers. The magnetic susceptibility of the both upper large model and lower small model is 1.81×10^{-1} (SI).
The magnetization intensity is 22.5 (A/m) with the inclination of 52.4 ° N and declination of 54.3 ° W. The thicknesses of the both models are equally 200 m.

11

Synthetic magnetic anomalies (Fig.8b) caused by a horizontal polygon model only with the mean magnetic susceptibility (8.16 x 10 $^{-2}$ SI) do not fit the observed anomalies (Fig.8a) at all. Synthetic magnetic anomalies (Fig.8c) caused by a horizontal polygon model with the mean magnetic susceptibility (8.16 x 10 $^{-2}$ SI) and remanent magnetization (6.15 A/m) do not fit the observed anomalies (Fig.8a) perfectly. Furthermore synthetic magnetic anomalies (Fig.8d) caused by the same model as Fig.8c except for 91.3 ° W in declination of Jn do not fit the observed anomalies (Fig.8a), either.

In order to fit synthetic anomalies to the observed, magnetic anomalies were calculated from two horizontal polygon models in layers (Fig.8e). In this case, the upper polygon model has the same horizontal dimension as that of Fig.8c with thickness of 750 m, while the lower one has smaller horizontal dimension than that of Fig.8c with thickness of 750 m under the northeastern part of the upper one. This implies that the complex is thicker in the northeastern part than in the southwestern part. Generally, this result is consistent with a geologic interpretation (OZAWA, 1984). However, the inferred thickness of the complex by the geologic interpretation ranges within several hundred meters.

If we assume the highest values of magnetic susceptibility (1.81 x 10 $^{-1}$ SI) and remanent magnetization (22.5 A/m) for the models, each thickness of the models is less than 200 m (Fig.8f). Although this result shows a better agreement with the geologic interpretation of the complex (OZAWA, 1984), such high magnetic susceptibility and magnetization intensity are rare in this study. Hence, Fig.8e is the most suitable interpretation for the magnetic anomalies of the MUC, at present.

5. Conclusion

We measured magnetic properties of the rock samples from the Miyamori ultramafic complex. The result shows a higher mean Qn ratio (1.90) than that of Kitakami granitic rocks (0.86). This means that we have to take account of remanent magnetization for analyzing magnetic anomalies caused by the complex. The result of the magnetic analyses based on the results of rock magnetic measurements shows that northeastern part of the complex is thicker than that of the southwestern part. In general, this result is consistent with a geologic interpretation of the complex. However, further rock magnetic studies are necessary for fixing a precise depth extent of the complex.

References

Japanese Association of Natural Gas (1986) Present Oil Exploration in Japan, 177.
Kawai, N., T. Nakajima and K. Hirooka (1971) J. Geomag. Geoelectr., 37, 1157.
NEDO (New Energy Development Organization) (1982) IGRF residual magnetic anomaly
    map, Morioka, Ichinoseki, scale 1 : 200,000.
Okuma, S. and H. Kanaya (1990) Chishitsu News, 428, 20.
Ozawa, K. (1984) Jour. Geol. Soc. Japan, 90, 697.
Ozawa, K.,K. Shibata and S. Uchiumi (1988) Jour. Japan Assoc. Min. Petr. Econ. Geol.,. Soc.
    Japan, 83, 150.
Seki, Y. (1951a) Jour. Geol. Soc. Japan, 57, 35.
Seki, Y. (1951b) Jour. Geol. Soc. Japan, 57, 217.
Talwani, M.(1965) Geophysics, 30, 797.
Yamada, N., Y. Teraoka, M. Hata (chief editors) (1982) Geological map, scale 1: 1,000,000.

MAGNETIC ANISOTROPY OF GNEISSOSE ROCKS OF SKARVSNES AREA, EAST ANTARCTICA.

Mutsumi NAKAI*, Minoru FUNAKI* and Peter WASILEWSKI**

*National Institute of Polar Research, Kaga1-8-10, Itabashi-ku, Tokyo, 173, Japan.
**Goddard Space Flight Center, Greenbelt. Maryland 20771, USA.

Introduction

It is difficult to obtain the significant NRM for paleomagnetism from metamorphic rocks, especially gneissose rocks, because of their gneissosity and their mineral alignments. As the gneissose rocks from Skarvsnes area, have well developed lineation of rock forming minerals, the NRM directions should be investigated whether the directions were reflected to the mineral lineation.

Skarvsnes area, 69.5°S latitude and 39.7°E longitude, is located in the east coast of Lützow-Holm Bay, Enderby Land, East Antarctica. This area is included the Lützow-Holm complex geologically, which is characterized by high temperature metamorphism called granulite facies. Various kinds of gneissose rocks are exposed for example, garnet-biotite gneiss, hornblende-gneiss, pyroxene-gneiss and metabasite (Ishikawa *et al.*, 1977). The geochronogical age of these rocks is estimated as about 500Ma(Nicolaysen *et al.*, 1961, Maegoya *et al.*, 1968) and before 1100Ma (Maegoya *et al.*, 1968, Shirahata *et al.*, 1983). Paleomagnetic samples are collected from 10 sites near the Mt.Suribati, the southern part of Skarvsnes area. They are gneissose rocks with clearly or unclearly defined lineation. The NRM was measured by a 3axes cryogenic magnetometer. Subsequently they are demagnetized up to 25mT by AF demagnetization. Subsequently residual NRM was thermally demagnetized at 180°C, 280°C and 330°C. The representative samples from the typical rocks were measured by the magnetic anisotropy by a VSM(Vibration Sample Magnetometer), in order to explain the relationship among the mineral lineation, magnetic anisotropy and the NRM direction.
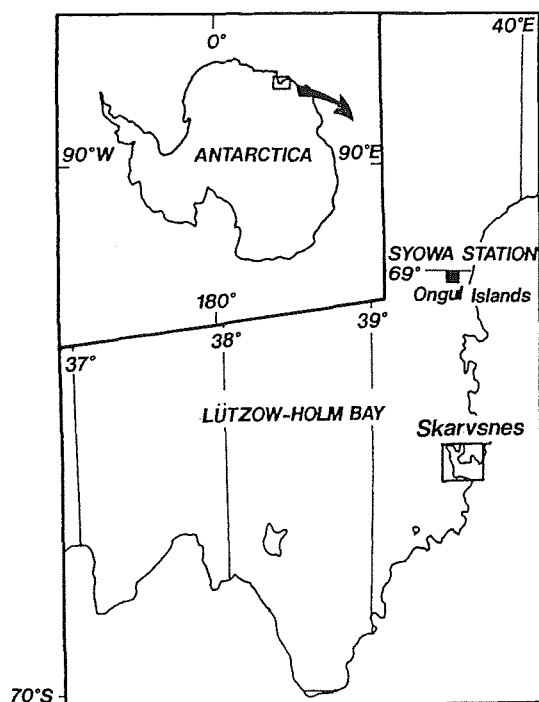

Fig.1 The location map of Skarvsnes.

Paleomagnetic result

The NRM directions of gneissose rocks from 8 sites are very scattered, even if they were treated by the magnetic cleaning (AF and thermal

demagnetization).

Fig.2 shows the orientation of the lineation by an arrow, with the original NRM directions(denoted (n) in figure) and after magnetic cleaning (denoted by solid and open circle) n:NRM, a:25mT AF demagnetization, t1:180°C,t2:280°C,t3:330°C thermal demagnetization. There is a tendency that the observed, NRM direction after cleaning turned to the fabric lineation of minerals. The NRM direction demagnetized by higher temperature(t2 or t3) resembled the orientation of lineation than that by lower temperature or AF demagnetization. Therefore, the NRMs of these samples were influenced by the lineation of gneissosity.

Some samples of gneissose rocks have negligibly weak lineation. They clustered at different 2 domains ((a) and (b) in the figure) and their Paleomagnetic data are shown in Fig.3. The VGP location obtained from the mean NRM direction of the cluster(b) consisted with the VGP-path of Gondwana Land (Thompson and Clark, 1982), at about 500Ma. However, that of the cluster (a) did not agree with the VGP-path path between Mesozoic and Paleozoic taking consideration of the α_{95} value.

Measurement of magnetic anisotropy

The basic magnetic properties, Hc(coercive force), Xi(initial susceptibility), Ir(saturate isothermal remanent magnetization), etc.were calculated from the hysteresis loop. The properties of a rock may vary by the applied field direction. In the case of gneissose rocks having clearly defined lineation, the anisotropy may be the strongest toward the orientation of lineation, therefore we measured hysteresis properties at every 15 degrees for the perpendicular 3 plains of X-Y plane, X-Z plane and Y-Z plane. In this paper, the anisotropy of the Hc, Xi and Ir values, were examined.

The samples with unclear fabric lineation of minerals, did not show significant amount of anisotropy for the Hc, Xi, and Ir values. The samples with well developed lineation have large anisotropy, for these values as shown in Fig.4.
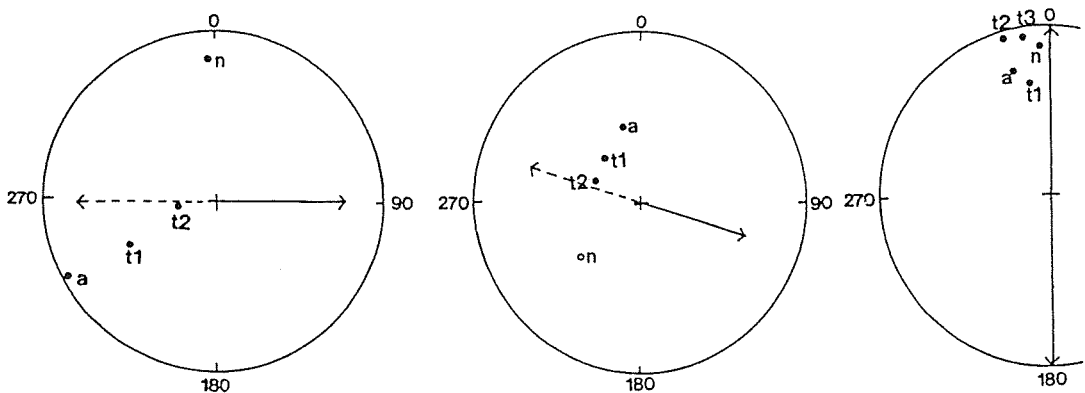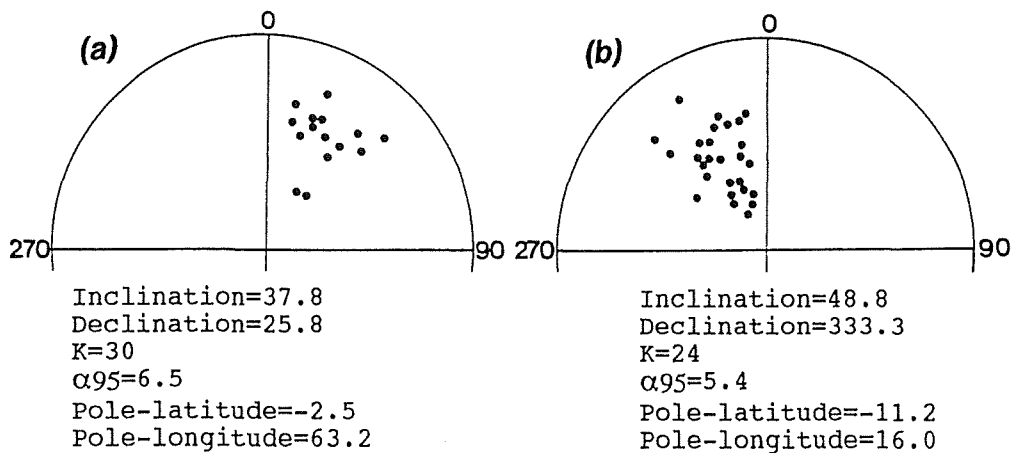

Fig.2 The direction of magnetic moment and the lineation of minerals.
The arrow:The lineation of minerals(The solid line is the upper sphere and the broken line is the lower sphere)
n:NRM, After magnetic cleaning-a:(AF-dema, 25mT)
t1,t2,t3:(Thermal-dema.180,280,330°C)

Inclination=37.8
Declination=25.8
K=30
$\alpha 95=6.5$
Pole-latitude=-2.5
Pole-longitude=63.2

Inclination=48.8
Declination=333.3
K=24
$\alpha 95=5.4$
Pole-latitude=-11.2
Pole-longitude=16.0

Fig.3 The paleomagnetic result of Skarvsnes.

The anisotropy of Hc was larger than that of the Ir and Xi. The maximum axis of anisotropy of Hc and Ir roughly agreed with the fabric lineation of rock forming minerals, but the minimum axis of anisotropy of Xi may be parallel with the lineation. The NRM direction after AF or thermal demagnetizations was shifted to the direction of the maximam anisotropy of axis of the Hc and Ir. Especially when the cleaning (t2)was applied to the sample more than the other cleaning(a, t1).

Mineral observation

Some stable magnetic directions are influenced with mineral lineation. It is satisfactory to consider the cause of the results as the lineation of magnetic minerals or mafic minerals including magnetic minerals. So, we measured the fabric orientations of mafic minerals in the samples as the magnetic direction. Then we studied the correlation between these orientations and the directions of the magnetic moment. Magnetite and ilmenite grains seemed in the matrix of the rocks and within the mafic minerals under the microscope. The orientation of these opaque minerals in the same sample always do not have the same direction, then some samples has over two large peaks of anisotropy of Hc and Ir values.

Discussion

The results obtained in this study agreed approximately with following expectation. The fabric lineation of rock forming minerals is related to the anisotropy of magnetic properties, as the Hc and Ir. Figure4 showed that the highest Hc appears toward the direction of fabric lineation. Therefore, it is considered that reliable NRM direction after optimum demagnetization is drown toward the fabric lineation of rock forming minerals rather than the ambient geomagnetic field direction when the rocks were metamorphosed.

These rock forming minerals essentially consist of the mafic minerals, but occasionally their orientations do not align to that of opaque minerals. The results can be explained that the mafic minerals order with magnetic minerals that are included them.

15
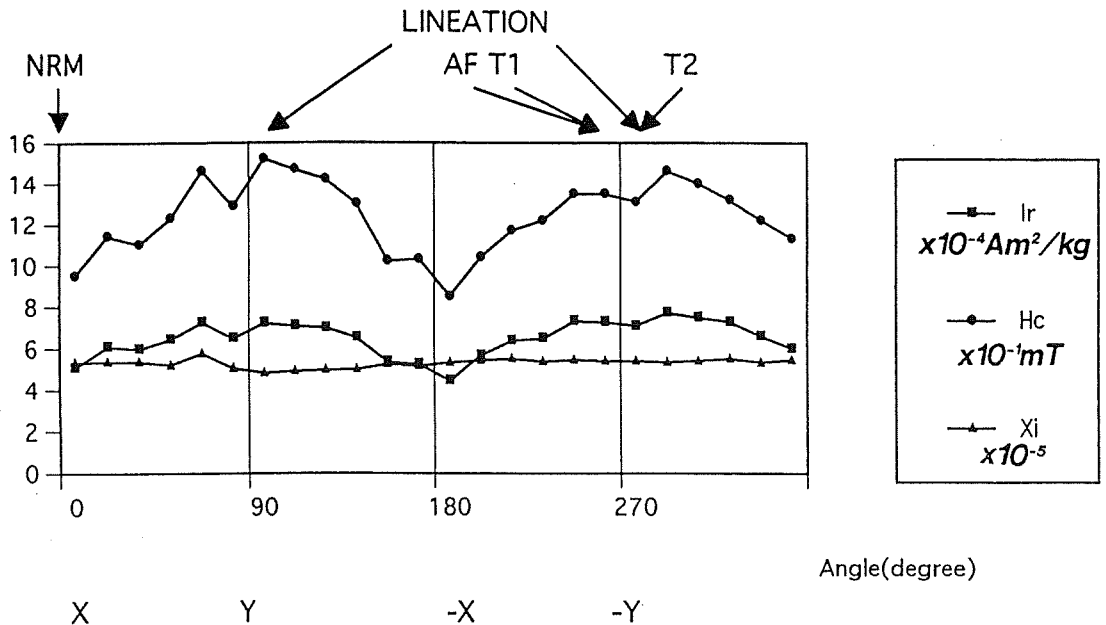
Fig. 4

Magnetic anisotropies of gneissose rocks from Skarvsnes(X-Y plane).

Without these data under the influence of the gneissosity, we can take the reliable paleomagnetic direction. It is the conclusion that the anisotropy of Hc and Ir is a useful method to check paleomagnetic data especially for gneissose rocks.

Hc has the biggest anisotropy of magnetic properties taken from a hysteresis. Xi has been used as method of anisotropy to find ordering of particles over the past years, but it seems to have less anisotropy than Hc and Ir in Fig.4.

The problem about measurement is that the curve of anisotropy in Fig.4 is not smooth. We think the reason of it is due to the heterogeneous of minerals in the rocks.

References

Ishikawa,T.*et al.*(1977), Antarctica Geological Map Series sheet 6 and 7 SKARVSNES. National Institute of Polar Research.
Maegoya, T. *et al.*(1968), Mem. Fac.Sci.,Kyoto Univ., Sci. Geol. Mineral., 35,131-138.
Nicolaysen,L.O. *et al.*(1961), Geochim. Cosmochim. Acta,22,94-98
Shirahata,H.(1983), Antarctic Earth Science, ed.by R.L. Oliver *et al.* Canberra, Aust. Acsd.Sci., 55-58.
Thompson,R and Clark,R. (1982), Earth Planet.Sci.Lett., 57 ,152-157.

TEMPERATURE DEPENDENT OF COERCIVITY FOR CHONDRITES, ALLENDE AND ALH–769

M. Funaki

National Institute of Polar Research, 9–10 Kaga 1, Itabashi Tokyo, 173, Japan

1. Introduction

Wasilewski (1981) reported the temperature dependent behavior up to 400°C of the magnetic coercivity of Allende (CV3) chondrite. His results elucidated that NRM blocking temperature (T_B) at 320°C in the thermal demagnetization curves was apparent due to a phase transition phenomenon analyzed by the temperature dependent of the coercive force (H_C) and remanent coercive force (H_{RC}). This experimental method seems useful for the estimation of carrier minerals of the NRM rather than the Curie point (Θ_{JS}) analysis in thermomagnetic (J_S–T) curves.

Occasionally the T_B temperature of meteorites is not harmonized with the Θ_{JS}, e.g. the NRM decayed 80% before 550°C but the J_S suddenly decayed at 760°C for Bocaiuva (IAB) iron meteorite (Funaki et al., 1988). This disagreements may commonly occur for the chondrites. Since the significant NRM should result from magnetic minerals with the high coercivity, the measurement of temperature dependent change of coercivity is more important for NRM analysis than for the Curie pont one. If samples include small amount of high coercive grains in a large amount of the low coercive matrix, identification of the magnetization resulting from the high coercive ones may be difficult in the J_S–T curves. In this study, the magnetic hysteresis properties (saturation magnetization J_S, saturation remanent magnetization J_R (SIRM), H_C, H_{RC} and initial susceptibility X_i) were measured during heating and cooling procedure for the Allende, and ALH–769 (L6) chondrites in order to find which parameter is more sensitive for the high coercivity grains.

The magnetic hysteresis loops were obtained between −1.4 and +1.4 mT of external magnetic field by a vibrating sample magnetometer with computer control. The samples were heated from 30° to 750°C with heating rate 50°C/h and cooling rate 100°C/h in 10^{-4} Pa atmospheric pressure. The loops were incessantly measured during the experiments with 20 minutes a cycle. The temperature changed about 16°C for the heating and about 32°C for the cooling in a cycle. The hysteresis properties, J_S, J_R, H_C, and X_i values were determined from the loop. The H_{RC} value was independently obtained from the loop. When the H_C value was smaller than 1mT, the H_{RC} was not measured because of worse precision. Although general magnetization in the J_S–T curves superpose ferro(ferri)magnetic and paramagnetic components, the J_S–T curves in this study show the ferro(ferri)magnetic component being subtracted the paramagnetic one. In this study, transition points appearing in the J_R–T, H_C–T, H_{RC}–T and X_i–T curves are denoted to Θ_{JR}, Θ_{HC}, Θ_{HRC} and Θ_{Xi} respectively.

2. Experimental results

Allende

The J_S–T curve of Allende (Fig. 1a) showed clearly defined large Θ_{JS} at 610°C and several small ones between 80°C and 350° in the heating curve. In the cooling curve, large Θ_{JS} at 610°C and small one at 290°C were observed. However, the determination of the minor Θ_{JS} in the heating curve is difficult whether they are significant or insignificant due to too small magnetization change. The Js=8.60x10^{-2}Am^2/kg of original sample increased to J_S=17.07x10^{-2}Am^2/kg after heating to 750°C.

The J_R–T curve (Fig. 1b) indicated the Θ_{JR} at 320°C and 560°C in the heating curve and at 590°C in the cooling curve. The original J_R=18.44x10^{-3} Am^2/kg decreased to J_R=4.23x10^{-3} Am^2/kg at 320°C in the heating curve and changed to J_R=10.46x10^{-3} Am^2/kg at 30°C after heat treatment.

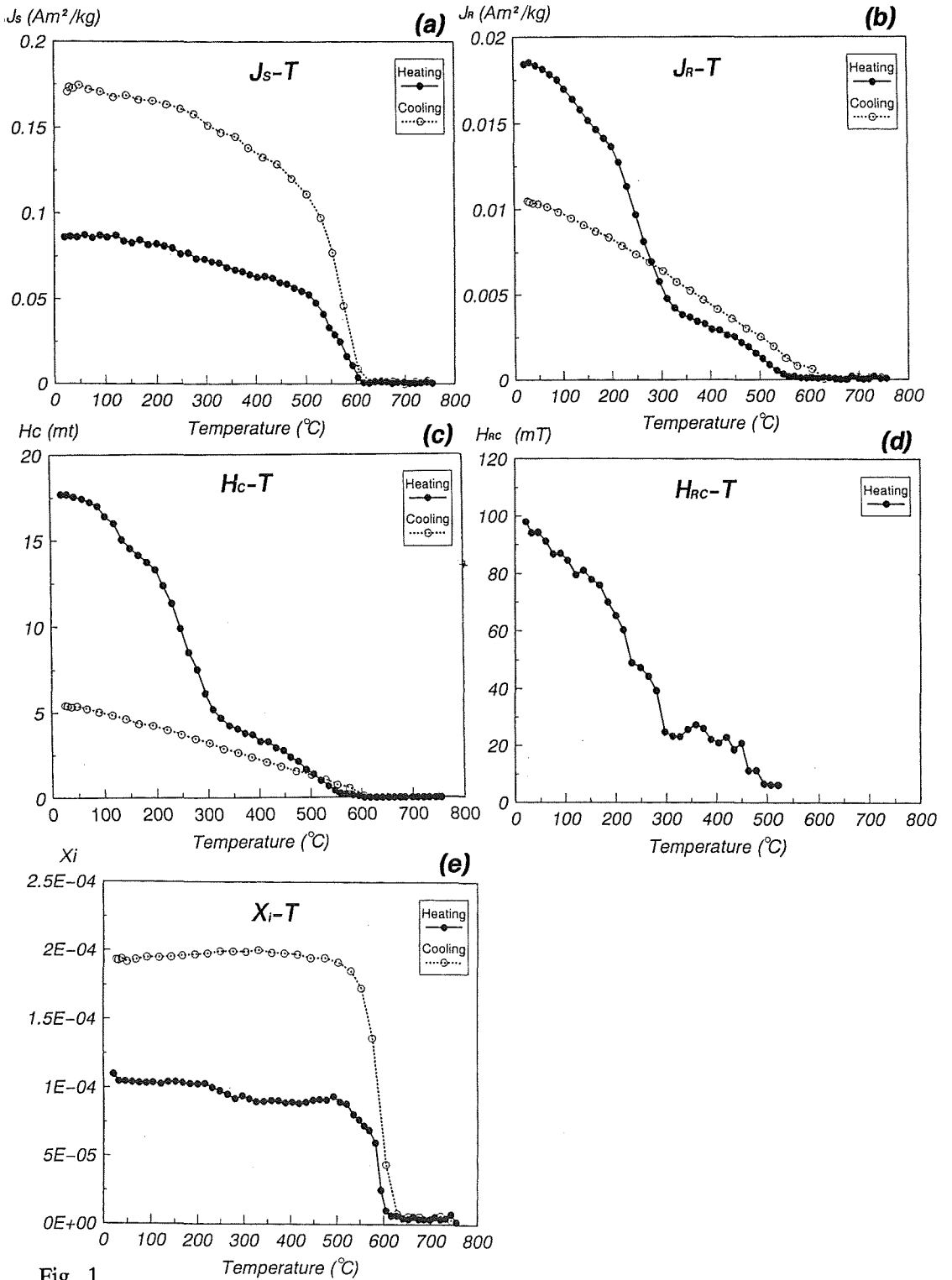Fig. 1
Temperature dependent of J_S, J_R, H_C, H_{RC} and X_i values for the Allende. (a):J_S–T curve, (b):J_R–T curve, (c):H_C–T curve, (d):H_{RC}–T, (e):X_i–T curve.

The H_C–T curve was very similar to the J_R–T one (Fig. 1c) with clear defined Θ_{HC} at 330° and 560°C, and minor one at 150°C in the heating curve, and the large Θ_{HC} at 590°C in the cooling curve. The original H_C=16.8 mT decreased to 4.7 mT at 330°C and 0.24 mT at 560°C. The H_C value after heating was 5.4 mT at 30°C.

Although the H_{RC}–T curve was unstable, the heating curve is shown in Fig. 1d. The H_{RC} value could not be measured in higher temperature than 525°C because of too small H_C values less than 1 mT. The reason of instability of the curve is estimated due to both of magnetic change and experimental precision of the H_{RC} measurements. However, temperature dependency of H_{RC} value can be roughly identified; the original H_{RC}=97.9 mT decreased to 23.1 mT at 320°C and Θ_{HRC}<10 mT at 500°C with the Θ_{HRC} at 245°, 320° and >500°C. A hump appeared between 300° and 400°C suggesting chemical alteration during the heat treatment.
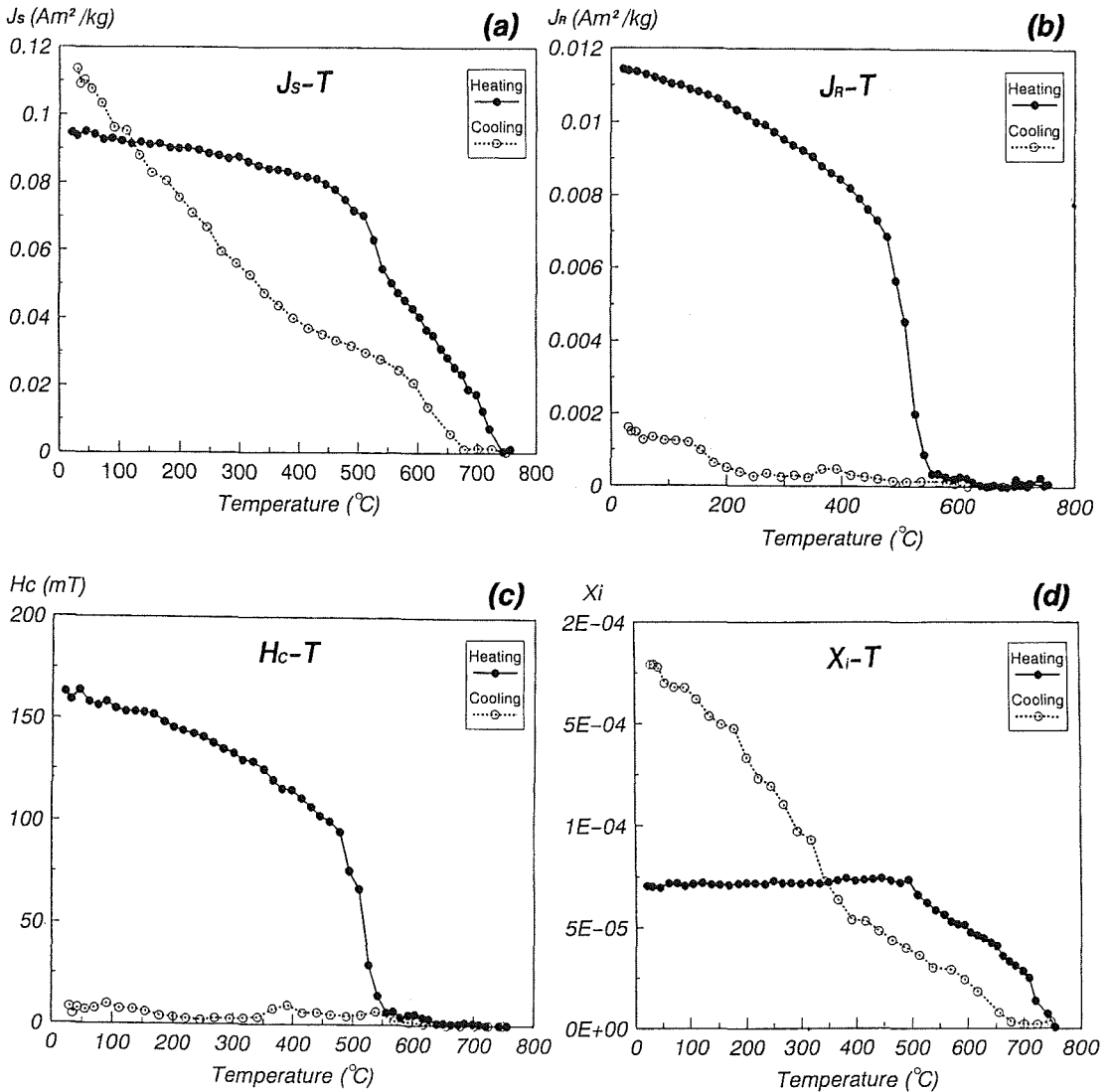

Fig. 2
Temperature dependent of J_S, J_R, H_C, H_{RC} and X_i values for the ALH–769. (a):J_S–T curve, (b):J_R–T curve, (c):H_C–T curve, (d):X_i–T curve.

The X_i–T curve gradually changed up to 500°C, and then abruptly decayed between 500° and 610°C in the heating curve and abruptly increased between 610° and 500°C in the cooling curve, as shown in Fig. 1e. The Θ_{Xi} was defined at 610°C for the heating and cooling curves associated with small ones at 280°, 360° and 420°C in the heating curve and at 445°C in the cooling curve. The original $X_i=1.098\times10^{-4}$ increased to 1.931×10^{-4} at 30°C after heat treatment.

ALH–769

The NRM intensity of ALH–769 (1.81×10^{-3} Am^2/kg) steeply decreased down to less than 1/5 of the initial value by AF demagnetization to 6 mT and then zigzag variation appeared. The thermal demagnetization results indicated that the NRM decayed steeply from 30°C to 200°C and gradually decreased from 200° to 500°C. The NRM higher than 500°C may be insignificant due to small magnetization and zigzag variation. The direction was relatively stable between 200° and 500°C, but it scattered widely at the both sides of the temperature range.

The J_S–T curve of ALH–769 (Fig. 2a) clearly defined Θ_{JS} at 550° and 745°C and minor one at 500° and 690°C etc. in the heating curve and 670° and 405°C in the cooling curve. The original $J_S=9.48\times10^{-2}$Am^2/kg increased to 11.37×10^{-2}Am^2/kg after heating to 750°C.

The J_R–T curve (Fig. 2b) showed one large Θ_{JR} at 560°C and small one at 640°C in the heating curve, and several small ones in the cooling curve. The original $J_R=11.43\times10^{-3}$Am^2/kg decreased to only 3% (3.54×10^{-4}Am^2/kg) at 560°C and negligibly small at 640°C in the heating curve. The value of $J_R=1.61\times10^{-3}$Am^2/kg appeared at 30°C after heat treatment.

The H_C–T curve (Fig. 2c) was very similar to the J_R–T curve; clearly defined Θ_{HC} at 560°C and minor one at 640°C in the heating curve and several unclear ones in the cooling curve were identified. The original $H_C=16.3$ mT decreased to 3.7% (0.6 mT) at 560°C in the heating curve. In the cooling curve, the H_C value appeared at 560°C and showed $H_C=0.86$ mT at 30°C after heat treatment.

The gradually decreasing H_{RC}–T curve was observed and the original $H_{RC}=122.7$ mT reached to an insignificant value at 560°C, although the curve was very noisy. In the cooling curve the value was not measured due to small H_C values less than 1 mT.

The X_i–T curve (Fig. 2d) showed almost flat curve from start to 500°C and then decreased gradually to $\Theta_{Xi}=755$°C in the heating curve with the small Θ_{Xi} at 570° and 670°. In the cooling curve, the X_i value appeared from 670°C with the Θ_{Xi} at 670°, 525° and 380°C. The original $X_i=7.03\times10^{-5}$ increased about 2.5 times (1.79×10^{-4}) by heat treatment.

Table 1. Basic data of the temperature dependent of hysteresis parameters.

meteorite	treatment	T_B	Θ_{JS}	Θ_{JR}	Θ_{HC}	Θ_{RC}	Θ_{Xi}
Allende	original	320°,≥600	610°	320°,560°, 150	330°,560°, 150	320°, 245,>500	610°,280, 335,420
	heated		610°,290, 400	590°	590°	–	610°,445
ALH–769	original	500°	550°,745° 500,690	560°,640	560°,640	560°	755°,570, 670
	heated		670°,405°	240,etc.	240,etc.	–	670°,525, 380
	Unit	°C	°C	°C	°C	°C	°C

*: main transition temperature, T_B: Curie point, Θ_{JS}: transition of J_S, Θ_{JR}: transition of J_R, Θ_{HC}: transition of H_C, Θ_{RC}: transition of H_{RC}, Θ_{Xi}: transition of X_i.

3. Discussion

Usually it is difficult to obtain the Θ_{JS} of high coercivity grains and/or alteration of the coercivity by the crystallin phase transition in the J_S–T curves, if the magnetic property of the grains satisfies the following either condition. (1) If a small amount of the high coercivity grain is present in the large amount of MD grains, the Θ_{JS} resulting from the high coercivity grains does not appear in the J_S–T curves due to large spontaneous magnetization by the MD grains. (2) If the coercivity changes by crystalline alteration by heating, the alteration cannot be detected in the J_S–T curves when the spontaneous magnetization is almost equivalent before and after the alteration. It may be also difficult to estimate the information of the high coercivity grains in the X_i–T curves. There is a possibility that the X_i–T curves show similar characteristics as the J_S–T ones, because spins in the MD grains can easily turn to the ambient applied field than SD ones. On the contrary, the H_C value shows the average coercivity of the sample and the H_{RC} value is drawn to the high coercivity grains (Nagata and Carleton 1987). The parameter of the J_R reflects the condition of coercivity of the H_C and H_{RC}. As the reliable NRM is carried by the high coercive grains, the analyses of the temperature dependent of J_R, H_C and H_{RC} values are more useful for analysis of NRM carrier grains than the J_S–T analysis.

The T_B and transition temperatures of the Allende and ALH–769 are summarized in Table 1. In the early stage of the magnetic study for the Allende an inconsistency was the Curie point at 320°C and the NRM blocking temperature at 600°C. This disagreement was explained by Wasilewski (1982) by the temperature dependent of J_S, H_C and H_{RC} values. He found out the clearly decreased H_{RC} value and small change H_C and J_S values at about 320°C, resulting from the chemical alteration. In case of the Allende, the above conditon (2) seems to be a reason of the disagreement between the T_B and Θ_{JS}. The results obtained in this study essentially support his results, although some differences appeared. His data indicated large change of the H_{RC} and small change of the J_S and H_C values at that temperature. In this study, large decay not only with H_{RC} but also with J_R and H_C values at 320°C appeared. However, any small transitions did not appear at 320°C in the J_S–T and X_i–T curves as described by Wasilewski (1982). As the Θ_{JS} at 320°C was only observed by Wasilewski, the inconsistency in the J_S–T curve is estimated that the chemical alteration is sensitively controlled by the experimental condition. The thermal demagnetization curve of Allende showed the almost 95% of NRM decay at 320°C. The temperature is completely consistent with the Θ_R, Θ_C and Θ_{HRC}. Therefore, the analysis of temperature dependent of the J_R, H_C and H_{RC} are more significant than that of J_S and X_i for estimation of the phase transition.

Magnetic mineral in the ALH–769 was identified to 65% of kamacite and 35% of plessite by Nagata (1979) and Funaki et al. (1981). The Θ_{JS} at 550°C of plessite is considered to be tetrataenite in present. The coercivity changed from large H_C=16.3 mT and H_{RC}=122.7 mT to small H_C=8.6 mT and H_{RC}<1 mT by the disorder under heat treatment and the feature of J_S–T curve are resemble to the magnetic change of tetrataenite to taenite. These characteristics may satisfy the identification of tetrataenite (Nagata and Funaki, 1986). The NRM of this chondrite decayed to almost 90% at 500°C by thermal demagnetization. The J_R and H_C values decreased to 5% at 560°C and to negligibly small at 640°C in the J_R–T and H_C–T curves. The T_B temperature differs away from the Θ_{JS} at 745°C of kamacite than that at 560°C of the disorder. From these viewpoints, the almost all stable NRM up to 560°C seems to be carried by tetrataenite. The phase transition at 565°C of tetrataenite was clearly defined in the J_S–T curve but it was less clear in the X_i–T curve. This reason is estimated that the X_i value of tetrataenite is extremely small by the high coercivity compared with that of kamacite of the low coercivity, while the spontaneous magnetization of tetrataenite appears in the J_S–T curve. Moreover, any magnetization of the taenite (produced from tetrataenite by disorder) did not appear in the temperature higher than 550°C by passing its Curie point. Consequently a clearly defined phase transition at 550°C in the X_i–T curve was not observed.

4. Conclusion

The characteristics of the temperature dependent of J_R, H_C and H_{RC} values give useful information for the analysis of the T_B resulting from high coercivity grains. As the J_R–T curve showed very similarity to the H_C–T curve, measurement of the temperature dependent of SIRM is useful for analysis of the high coercivity grains. However, it is difficult to take the information of the grains from the J_S–T and X_i–T curves, when the amount of that grains are small.

References

Funaki, M., Nagata, T. and Momose, K. (1981) ALH–769. Men. Natl Inst. Polar Res. Spec. Issue, **20**, 300–315.

Funaki, M., Taguchi, M., Danon, J., Nagata, T. and Kondo, Y. (1988) Proc. NIPR Symp. Antarc. Meteorites, **1**, 231–341.

Nagata, T. (1979): Phys. Earth Planet. Inter., **20**, 324–341.

Nagata, T. and Funaki, M. (1986): Mem. Natl Inst. Polar Res., Spec. Issue, **46**, 245–262.

Nagata, T. and Carleton, B.J. (1987): J. Geomag. Geoelectr., **39**, 447–461.

Wasilewski, P. (1981): Phy. Earth Planet. Int., **26**, 134–148.

Wasilewski, P.J. (1982): Lunar and Planetary Science XIII. Houston, Lunar Planet. Inst., 843–844.

SPELEOTHEM AND KARST ENVIRONMENT*

Yuyan LIU(1), Hayao MORINAGA(2) and Katsumi YASKAWA(3)

1 China University of Geoscience, Yujia Hill, Wuhan 430074,
People's Republic of China
2 Faculty of Science, Himeji Institute of Technology, 2167 Shosha,
Himeji 671-22, Japan
3 Faculty of Science, Kobe University, 1-1 Rokkodai-cho, Nada, Kobe 657, Japan

Introduction

Karst speleothems are formed, after caves rise above the surface of the ground water, through the reaction of vadose water and CO_2, and also through the precipitation and crystallization of corroding limestone liquid. As far as their types are concerned, speleothems are classified into dripstones, flowstones, the deposits of water concentration, etc. On the other hand, the calcites formed by water dripping in the cave can be further grouped into such typical shapes as stalagmites, stalactites, stalacto-stalagmites, calcareous slates, etc. Among them, stalagmites, growing upwards, have always been the researcher's favorites because of their simple construction and the convenience of their collection.
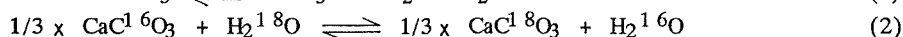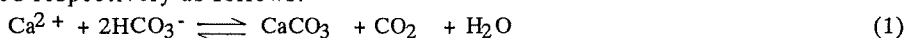
The proportion of the chemical composition of stalagmites and the precipitation rate

The main composition of the stalagmites includes CaO, MgO, SiO_2, Al_2O_3 and FeO. Among them, CaO and MgO are soluble oxides and the other three are insoluble. The elements of the above-mentioned oxides mainly derive from the element providing vadose water from the surface soils and the limestone bodies through which the vadose water passes. These oxides undergo a slow process of crystallization and mineralization in the cave under normal temperature and pressure, and open system. Therefore, by determining the chemical composition of the stalagmite, we can know not only the source of each element of the stalagmite (each element derives from the content proportion of the surface soil and the limestone), but, what is more important; the proportion variation pattern during the stalagmite growing period.

Generally speaking, the content of the soluble oxides of the stalagmite is often lower than that of the mother limestone, while the content of the insoluble oxides is otherwise. This content difference is caused by the fact that the insoluble surface earth (mainly composed of oxides) was brought into the stalagmite by vadose water through the cracks of the limestone bodies. Thus, the variation of the content proportion of the soluble oxides to the insoluble ones reflects the variation of the vadose water or cracks of the limestone bodies. If the strata cracks are considered to be caused by sheer corrosion, and the vadose water, related to corrosion, comes from rainfalls, the variation of content proportion of the chemical composition in the stalagmite growing period reflects the variation of precipitation in that period. Generally speaking, an increase of the soluble oxides and a decrease of the insoluble oxides reflect a decrease in precipitation. Conversely, a decrease of the soluble oxides and an increase of the insoluble oxides reflect an increase in precipitation.

The isotope of the stalagmite and paleotemperature

The chemical equation of the stalagmite growth and its isotope exchange equation are presented respectively as follows:

$$Ca^{2+} + 2HCO_3^- \rightleftharpoons CaCO_3 + CO_2 + H_2O \qquad (1)$$

$$1/3 \times CaC^{16}O_3 + H_2^{18}O \rightleftharpoons 1/3 \times CaC^{18}O_3 + H_2^{16}O \qquad (2)$$

As the isotope theory points out, if the above-mentioned isotope exchange occurs under a chemical equilibrium (i.e. there is no kinetic fractionation), and the stalagmite has been in a closed state and has not been altered by the later vadose water, we can obtain, according to the experimental formula (O'Neil et al., 1969), the absolute value or relative variation of the paleotemperature of the district and the period in which the stalagmite grew, by the determination of the stalagmite's $\delta^{18}O$ and the enclosure water's $\delta^{18}O$, or by the determination of the stalagmite's $\delta^{18}O$ alone. Generally speaking, when high $\delta^{18}O$ of the stalagmite arises, the temperature is low. Conversely, when the low $\delta^{18}O$ arises, the temperature is high.

However, the problem is whether the isotope exchange reaction goes under an equilibrium through the whole process, about which Hendy (1971) pointed out two judging principles:

(1) The stalagmite's $\delta^{18}O$ of the same growth layers is identical;

(2) The stalagmite's $\delta^{18}O$ and the $\delta^{18}O$ of different growth layers are irrelative.
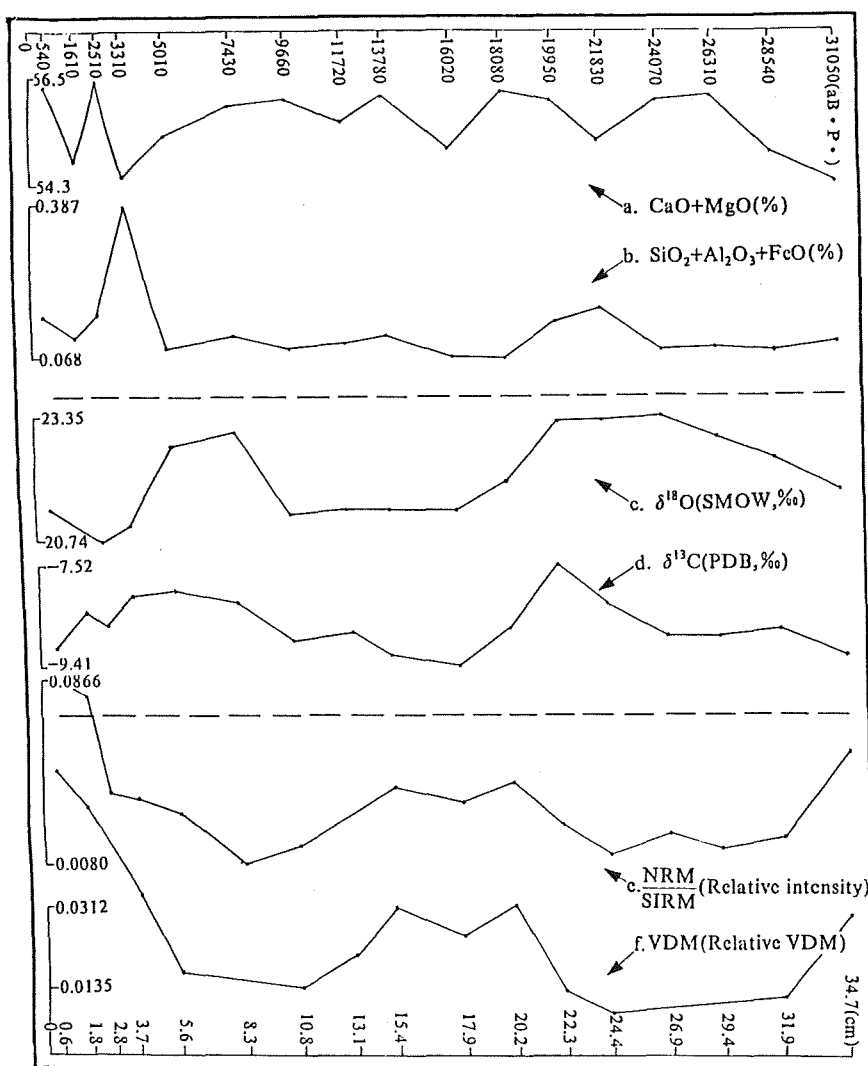

Fig. The results of the chemical composition, isotope of oxigen and carbon, and paleomagnetic field intensity of the stalagmite from Shihua Cave, Beijing.

According to the principles, only the $\delta^{18}O$ in question can reflect paleotemperature. The authors have made a study on the $\delta^{18}O$ of the same layers in stalagmites from Hubei and Shaaxi provinces, and the statistical results show that, if there are no obvious stratohorizon error and error of determination, the error of mean square of most of the same growth layers is less than +-0.1 permil of the experimental error. Thus, the second principle stated above is more important.

The magnetic features of the stalagmite and the paleomagnetic field

Stalagmites possess the following magnetic features (Morinaga et al., 1989: Latham et al., 1989):

    (1) Its remanent magnetization is being developed while $CaCO_3$ is crystallizing;

    (2) It possesses stable remanent magnetization;

    (3) It records the variation of the paleomagnetic field as it really is;

    (4) It is not affected by the shape and declivity.

The stalagmite's magnetization, the authors believe, occurs , when $CaCO_3$ is undergoing a slow crystallization, the magnetic minerals in the vadose water made a directional alignment in the direction of the geomagnetic field. This magnetization is depositional remanent magnetization accompanying the process of crystallization. This remanent magnetization can be used not only to find out the declination and inclination of the geomagnetic field, the virtual geomagnetic pole, the intensity of the field, and the variation of the magnetic moment of the virtual dipole, but to discover various special events of paleomagnetic field as well, including polarity reversal and drift.

Illustration

The stalagmite was collected from Shihua Cave in Fangshan District, Beijing. EPM-810Q electron probe microanalyzer, MAT-251 mass analyzer and SCT SQUID magnetometer were used respectively to determine the stalagmite's chemical composition, isotope composition of oxygen and carbon, and remanent magnetization. The root part age of the stalagmite, according to the ^{14}C age determination, is 31,050 years BP. Figure is the results of the determination. the horizontal line at the bottom indicates the distance between the central part and the top of the sample. VDM refers to the magnetic moment of the virtual dipole deduced from NRM/SIRM (indicator of relative intensity of the geomagnetic field).

    From the figure, we should know:

    (1) There were two periods when the precipitation increased (suggesting from a decrease of the soluble oxides and an increase of the insoluble oxides) and the paleotemperature rose (suggesting from the stalagmite's $\delta^{18}O$ decrease) in the area of Beijing since 31,050 years BP, respectively.

    (2) There were also two periods when the VDM increased. Paleotemperature and paleomagnetic field intensity have a positive correlation, but the latter changes prior to the former.

References

Hendy, C (1971) Geochimica et Cosmochimica Acta, 3 5, 801.

Latham, A. G., D. C. Ford, H. P. Schwarcz, and T. Barchall (1989) Phys. Earth Planet. Inter., 5 6, 34.

Morinaga, H., H. Inokuchi, and K. Yaskawa (1989) Geophys. J., 9 6, 519.

O'Neil, J. R., R. N. Clayton, and T. K. Mayeda (1969) J. Chem. Phys., 5 1, 5547.

FIELD-STRENGTH DEPENDENCE OF DIRECTIONAL DISPERSION IN MAGNETIZATIONS OF SEDIMENT SAMPLES : A STATISTICAL MODEL AND PALEOMAGNETIC EVIDENCE

Masayuki HYODO[1] and Chizu ITOTA[2]

[1] Department of Earth Sciences, Faculty of Science, Kobe University, Kobe 657, Japan
[2] Department of Earth Science, Nihon University, Setagaya, Tokyo 156, Japan

A statistical model is proposed for alignments of magnetic moments in a sediment controlled by the strength of the geomagnetic field. The model predicts that both of the mean intensity and directional convergence of magnetizations in sediment samples are dependent upon the strength of the geomagnetic field (Table 1). This prediction was examined with the paleomagnetic data from wide-diameter cores of marine and lacustrine sediments in Japan. The magnetization of a core from the Inland Sea shows a positive correlation between the depth-dependency changes in mean intensity and the Fisher's precision parameter, k, which is a measure of the clustering of directions at the same age horizon. For cores from Osaka Bay and Lake Yogo, the similar correlation can be recognized in the high frequency components. The time-dependency variations of k of these three cores are consistent with each other. Besides, these variations seem to have tight correlation with the secular variation of the geomagnetic field strength from the archeomagnetism (Fig.1). This suggests that the parameter of directional convergence degree can be used as an estimator of relative paleointensity. On the other hand, the data of these three cores show no correlation of the time-dependency variation of natural remanent magnetization intensity even after normalization using saturation isothermal remanent magnetization. This disagreement may be due to alterations of grains' moments by some effects of diagenesis (Karlin, 1990) or to difficulty in normalization of quantity of effective magnetic moments.

The relative paleointensity for the last 12000 years estimated from the directional convergence variation (Fig.1) is prominently characterized by a high peak at 2000 - 3000 years BP and a minimum at 5500 - 6000 years BP. This estimation of the paleointensity in Japan is similar to the archeomagnetic paleointensity in Europe (Kovacheva, 1980), suggesting that they should be originated from the nature of dipole field. The MEM spectral analysis indicates spectral peaks at periods of 4000, 1100, 770 and 590 years per cycle. The periodicities of 7000 years, pointed out in a previous work (Tanaka, 1991), and about 2000 years of the westward-drift are not found in the present analysis.

Table 1. Relationships of various parameters between populations a and b expected from the model. The population a shows a distribution of magnetic vectors aligned in a field strength of f_a and the population b in f_b. The lower three parameters are observable in paleomagnetism.

Parameters	Order of magnitude		
Field strength	f_a	<	f_b
Population variance of direction vectors	σ_a^2	>	σ_b^2
Sample variance of direction vectors	s_a^2	>	s_b^2
Precision parameter	k_a	<	k_b
Magnetization intensity	M_a	<	M_b

Precision parameter v.s. Age

Paleointensity
in Europe

Osaka Bay   Lake Yogo   The Inland Sea

Calibrated Radiocarbon Years (Ka)
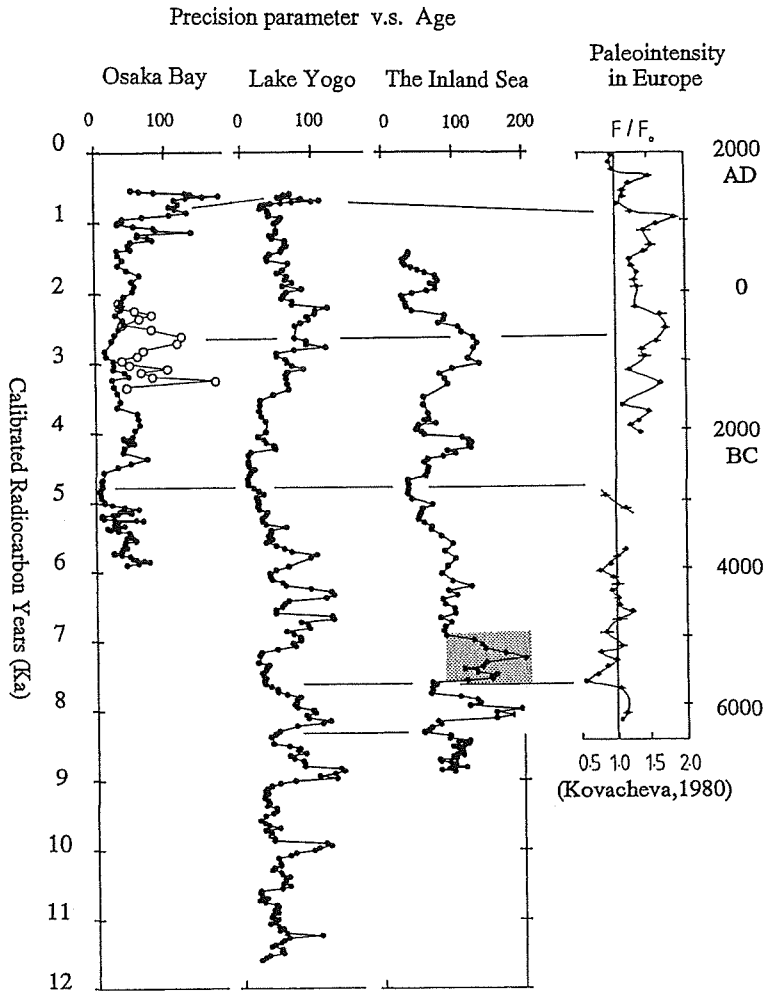
Fig.1 Comparison of the time-dependence plots of precision parameters from Osaka Bay, Lake Yogo and the Inland Sea, and the secular variation of paleointensity by archeomagnetism. The open circles in the plot of Osaka Bay show the precision parameters calculated from 4-5 magnetization directions in each horizon. The shaded portion in the plot of the Inland Sea represents the discrepancy from the values of Lake Yogo. The secular variation of paleointensity, based on the Thellier method using TRM's (right), is from Bulgaria (Kovacheva, 1980).

References

Karlin, R. (1990), J. Geophys. Res., 95, 4405-4419.
Kovacheva, M. (1980), Geophys. J. R. Astron. Soc., 61, 57-64.
Tanaka, H. (1991), J. Geophys. Res., 95, 17517-17531.

(In press in J. Geomag. Geoelectr.)

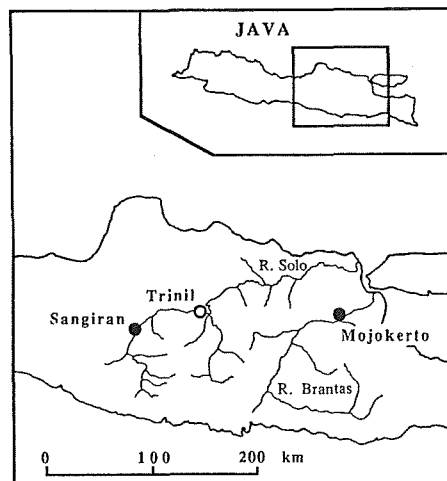# MAGNETOSTRATIGRAPHY OF HOMINID FOSSIL BEARING FORMATIONS IN SANGIRAN AND MOJOKERTO, JAVA

Masayuki Hyodo[1], Naotune Watanabe[2], Wahyu Sunata[3], Eko Edi Susanto[3], and Hendro Wahyono[3]

1 Department of Earth Sciences, Faculty of Science, Kobe University, Nada, Kobe 657, Japan.
2 Kohinata 2-24-17, Bunkyou , Tokyo 112, Japan.
3 Geological Research and Development Centre, Jl. Diponegoro 57, Bandung, Indonesia.

Paleomagnetic investigation of Plio-Pleistocene formations in Sangiran and Mojokerto, Java (Fig.1) was carried out to date stratigraphic levels of Pithecanthropus fossils. Secular variation records of paleomagnetic field direction from the two areas show very consistent changes. The most prominent feature obtained at the two areas is a long-term geomagnetic excursion between the Jaramillo and the Olduvai events, which is characterized by a large westerly deflection of field direction (Hyodo et al., 1992). Another feature is the dominance of easterly and downward directions during the Jaramillo and Olduvai events. These features enabled us to correlate the paleomagnetic records from the two areas (Fig.2). The record for the past 3 million years obtained in Sangiran reveals nine polarity boundaries from the upper boundary of the Mammoth event to the Brunhes/Matuyama boundary. The result revises the magnetostratigraphy of earlier investigations (Yokoyama, 1980; Semah, 1982; Shimizu, 1985). Based on correlation of the secular variation record of Mojokerto with that of Sangiran, magnetostratigraphy of Pleistocene formations in Mojokerto was established.

The stratigraphic zone of *Pithecanthropus* in Sangiran ranges from the lower boundary of Jaramillo event to the Brunhes / Matuyama boundary, and the stratigraphic level of *Homo modjokertensis* lies at the lower border of Jaramillo event. Magnetochronologically it dates from about 0.73-0.97 m.y. for Sangiran and about 0.97 m.y. for Mojokerto. The latter date is the first clear evidence to reject the former absolute age of 1.9 Ma by K-Ar dating for *Homo modjokertensis* (Jacob, 1972) whose reliability has been disputed for a long time.

Fig. 1   Location of Sangiran and Mojokerto, the investigated areas, and Trinil, the discovery site of Pithecanthropus fossils by Dubois.

SANGIRAN

MOJOKERTO

LITHOLOGY

Polarity

DECLINATION

DECLINATION

Polarity

LITHOLOGY

Fission
track age

-90 0 90 180 270°

-90 0 90 180 270

Notopuro F.
(Pohjajar F.)

Upper
Lahar

Kabuh F.
(Bapang F.)

Upper T.
Middle T.
Lower T.
Grenzbank
Zone

Pucangan Formation
(Sangiran Formation)

T11
T10
T9
T8
T7
T6 T5
T4 T3
T2
T1

Lower
Lahar

Balanus
Limestone

Upper T.

Kalibeng Formation
(Puren Formation)

Nodule
Middle T.
Lower T.4
Lower T.3
Lower T.3
Lower T.1

Marine | Lagoonal

Hominid fossils

0.25
0.49 *
0.58 *
0.71
0.71
0.78

1.16

1.49
1.51

2.48

2.92
2.99

(Myr)

0.73

0.90
0.97

1.67
1.87
?

3.01
3.05

Gravel bed
Sand &
gravel SG5

Sand &
gravel SG4

S. & gravel SG3

Mollusc. III ML3

Sand pipe SP

S. & gravel SG2
SG1

Molluscan
Horizon II ML2

Kabuh Formation

Pucangan Formation

Marine | Fluviatile

(Myr)

0.73

0.90
0.97

1.67

Hominid fossil

-?-

-?-

A
B

Silty   Sandy

Alteration of sand
& tuffaceous sand

A, B *Homo modjokertensis* (see Fig.10)

Vertebrate fossils

Levels paleomagnetically corresponding
to Formation-boundaries in Sangiran
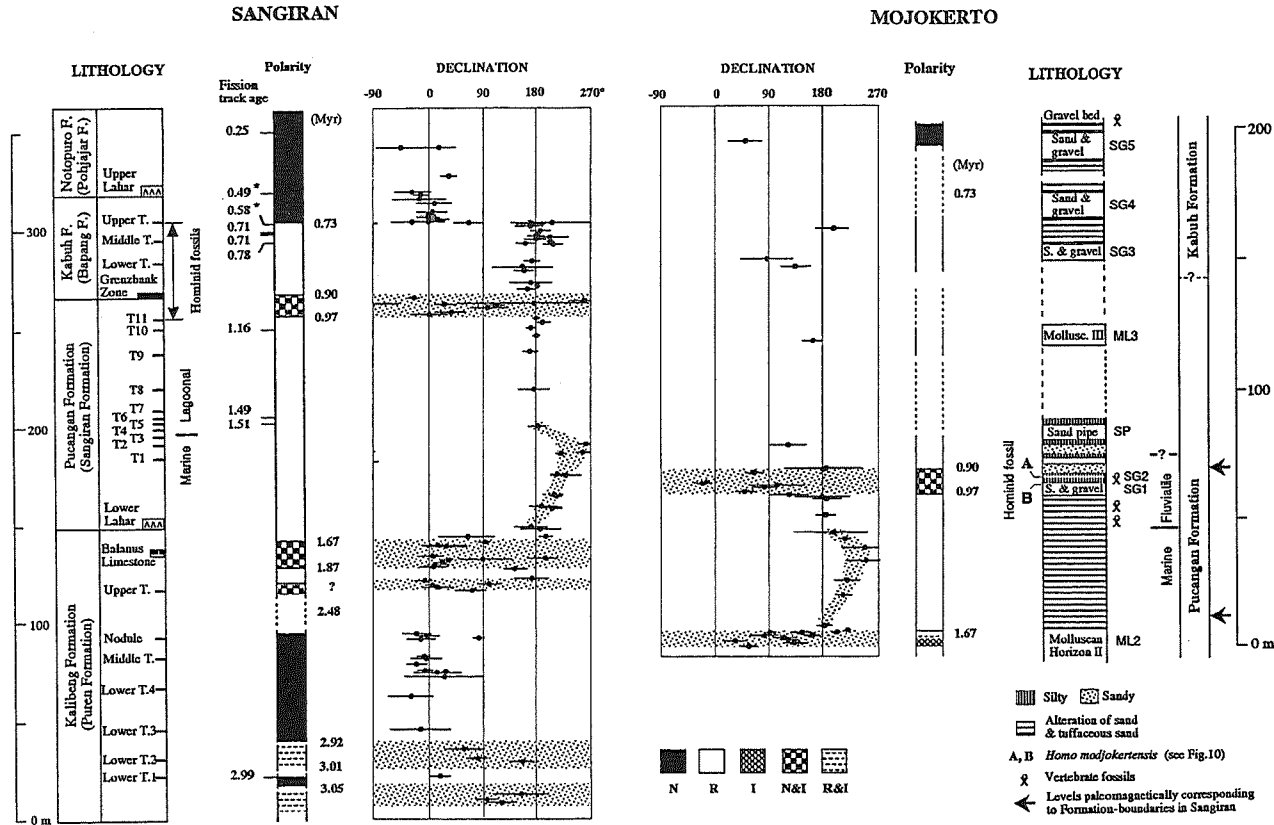
N   R   I   N&I   R&I

Fig. 2   Magnetostratigraphy and declination plot for Sangiran and Mojokerto. Shaded portions in the declination plot show mixed polarity zones and a long sequence of westerly rotated fields. On the polarity column of Sangiran, fission track ages with an asterisk are after Suzuki (1985) and those without asterisk after Suzuki et al. (1985). On the geological column of Mojokerto, A and B indicate the find level of *Homo modjokertensis* : A after Kumai et al. (1985) and B after Jacob (Personal communication). Two arrows at the extreme right indicate the levels paleomagnetically correlating to the Formation boundaries in Sangiran: upper arrow shows the Pucangan (Sangiran)/Kabuh (Bapang) boundary and lower arrow the Kalibeng (Puren)/Pucangan (Sangiran) boundary.

References

Hyodo, M., W. Sunata and E.E. Susanto (1992) J. Geophys. Res., 97, 9323-9335.

Jacob, T. (1972) Antiquity, 47, 148

Kumai, H., M. Itihara, Sudijono, Shibasaki, T., F. Aziz, S. Yoshikawa, S. Akahane, T. Soeradi, T. Hayashi and K. Furuyama (1985) *Quaternary geology of the hominid fossil bearing formations in Java* (Watanabe, N. and Kadar, D., ed.), Geol. Res. Dev. Centre, Spec. Publ. 4, pp. 55-61.

Semah, F. (1982) *Mod.Quaternary Res. SE Asia* ,7, 151-164.

Shimizu, Y., B. Mubroto, H. Sigagian and M. Untung (1985) *Quaternary geology of the hominid fossil bearing formations in Java* (Watanabe, N. and Kadar, D., ed.), Geol. Res. Dev. Centre, Spec. Publ. 4, pp. 275-308.

Suzuki, M. (1985) *J. Anthr. Soc. Nippon* 93, 197. (in Japanese)

Suzuki, M., Wikarno, Budisantoso, I. Saefudin and M. Itihara (1985) *Quaternary geology of the hominid fossil bearing formations in Java* (Watanabe, N. and Kadar, D., ed.), Geol. Res. Dev. Centre, Spec. Publ. 4, pp. 309-357.

Yokoyama, T., S. Hadiwisastra, A. Hayashida and W. Hawtoro (1980) *Physical Geology of Indonesian Island Arcs* (Nishimura, S., ed.), Kyoto Univ., pp. 88-96.

(In press in Anthropological Science)

PALEOMAGNETISM OF THE DRILLING CORE SAMPLES IN LAKE NOJIRI, NAGANO PREFECTURE, CENTRAL JAPAN

Paleomagnetic Research Group for Nojiri-ko Excavation

c/o Nobuyuki AIDA, Sawara Senior High School, Sawara city, Chiba 287

Introduction

Lake Nojiri is a beautifull lake in Shinano-machi, Nagano Prefecture, central Japan, 654 meters above sea level with a maximum depth of 38.5m. It is surrounded by four Pleistocene stratovolcanoes, Myoko, Kurohime, Iizuna and Madarao.

The Nojiri-ko Excavation has been carried out since 1962 to restore natural environment around Lake Nojiri where Palaeolithic men lived in the Last Glacial Age. Main excavations were carried out at Tategahana on the west shore of the lake.

In 1988, drilling by Geological Survey of Japan was performed at the site of -28.9m in depth, 700m south-east of Tategahana (Fig.1), and a 45.1m core sample was obtained.

Geology

A 45.1m core sample was formed of mudflow (depth: 45.10-44.08m) and unconsolidated sediments above it. The unconsolidated sediments consist of peat (depth: 44.08-33.98m), silty clay (depth: 33.98-0.63m) and ooze (depth: 0.63-0m) in ascending order. Based on tephrochronology of the sediments, five stratigraphic units are identified as Table 1: Biwazima-oki Peat Member, Kannoki Formation, Nojiri-ko Formation, J-retsu Formation and Recent lake deposits, the every unit being conformable to each other.
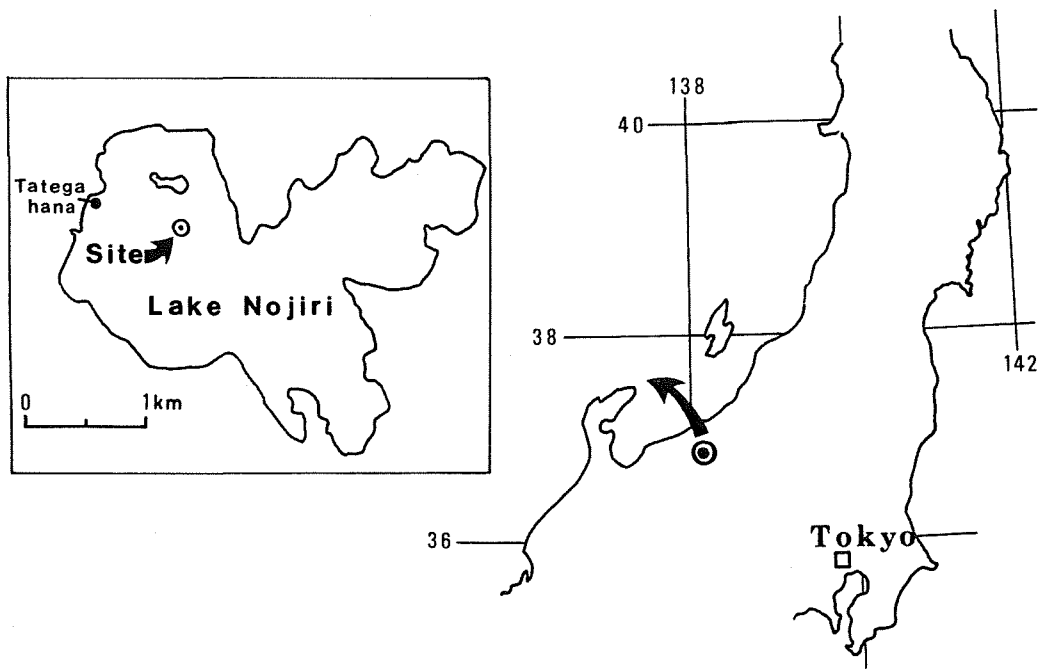
Fig. 1 Map showing the site of the drilling core

Table 1 Stratigraphic succession of the drilling core

STRATIGRAPHIC DIVISION[1]			DEPTH[1]	[14]C DATING[2]
Recent lake deposits			0 ～ 0.63 m	
J-retsu Formation			0.63～ 7.83 m	8000～11000 y.B.P.
Nojiri-ko Formation	Upper	Ⅱ・Ⅲ	7.83	11000～33000
		Ⅰ	～16.21 m	33000～39000
	Middle		16.21～17.27 m	39000～41000
	Lower Ⅲ・Ⅱ・Ⅰ		17.27～28.90 m	(Ⅲ) 41000～49000
Kannoki Formation			28.90～33.98 m	
Biwazima-oki Peat Member			33.98 ～44.08 m	
Mudflow			44.08～45.10 m	

※1: Geology Research Group for Nojiri-ko Excavation (1990)
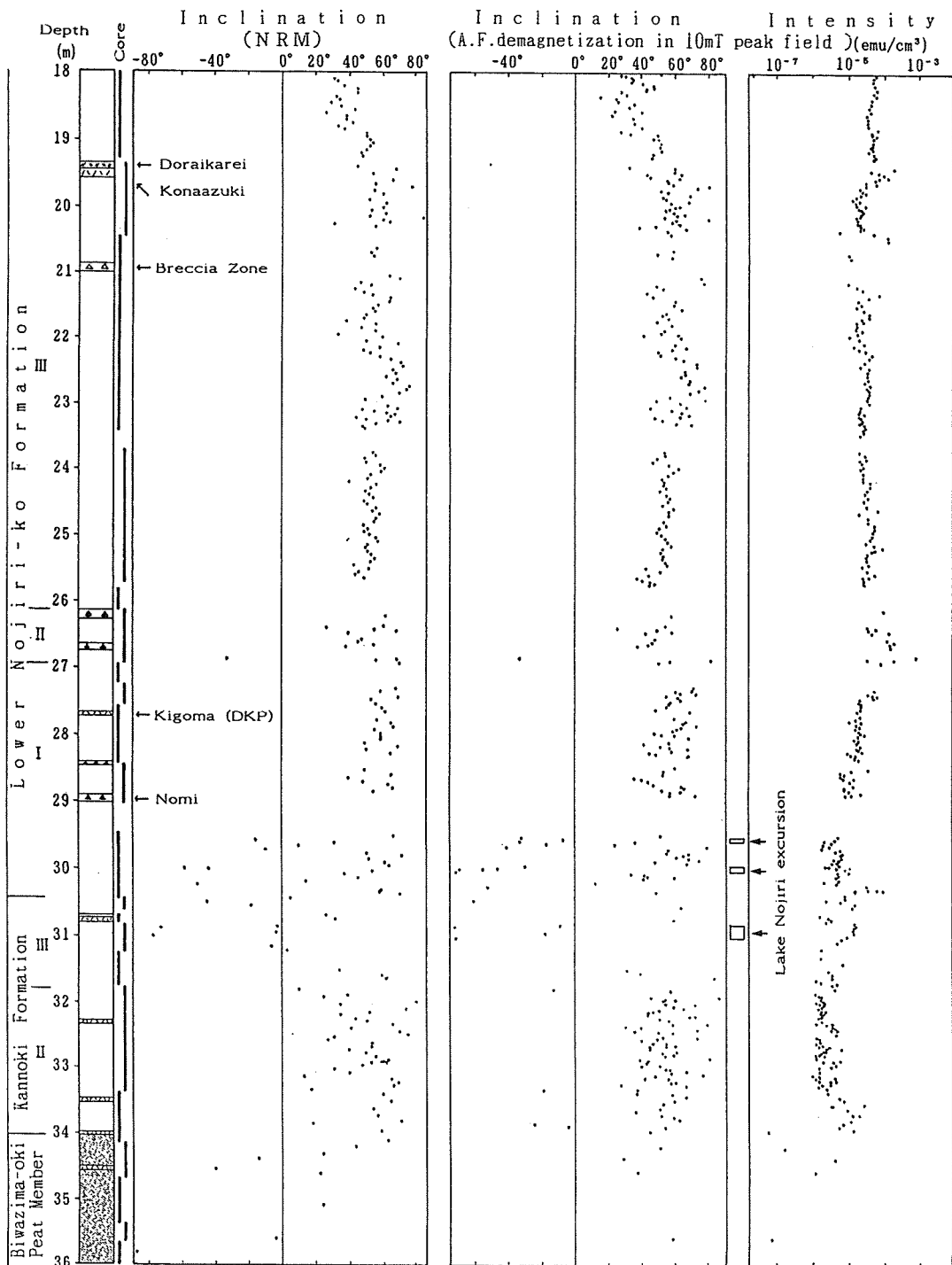
2: Sawada et al.(1992)

Fig. 2 The result of magnetic measurements of the
drilling core (depth: 18-36m)

Paleomagnetism

    1100 samples for paleomagnetic analysis were mainly taken
from silty clay of Kannoki and Nojiri-ko Formation. All the
specimens were put in cubic capseles 2.4cm on a side made by
polycarbonate.

    All the specimens were demagnetized in alternating
fields(A.F.) in 10mT, based on the stability tests of
stepwise A.F. demagnetization.

    Almost of all the specimens are normally magnetized,
except for the specimens of Lower Nojiri-ko Formation I and
Kannoki Formation III , 29.5-31.25m in depth (Fig.2).

    The dates of Nojiri-ko Formation at Tategahana were
obtained from ^{14}C measurements with a Tandetron accelarator
mass spectrometer (Sawada et al.,1992). As ^{14}C ages of the
lowest part of the Lower Nojiri-ko Formation III is 49410±970
y.B.P., the age of the reversely magnetized specimens of 29.5-
31.25m in depth will be supposed to be a little greater than
50000 yr. This reversal may be observed in three horizons as
shown in Fig.2, probably corresponds to the geomagnetic
excursion named "Lake Nojiri excursion" in the Brunhes epoch.

                        References

Geology Research Group for Nojiri-ko Excavation (1990)
     Monograph Assoc.Geol.Collab.Japan, 37, 15.
Sawada,K., Y.Arita, T.Nakamura, M.Akiyama, T.Kamei and N.Nakai
     (1992) Earth Science(Chikyu Kagaku), 46, 133.

        (To be published in Monograph Assoc.Geol.Collab.Japan)

Paleomagnetic study of the Yusenkyo Formation,eastern Hokkaido

Toshiya Kanamatsu

Ocean Research Insitute, University of Tokyo

INTRODUCTION

Hokkaido is regarded as the place where two arcs have collided from Miocene time (Kimura,1986). A number of reconstruction models of two paleo-arcs in the Cretaceous time before collision tectonic event, has been presented (Niida and Kito,1986 and many others)

One of two arc-trench systems in Cretaceous time was the Paleo-Japan arc-trench system, with westward subduction under the Eurasian plate.

Evidences of westward subducting of Cretaceous Japan arc-trench system are occurrences of the high pressure type metamorphic rocks, products of volcanics and melanges (Niida and Kito,1986).

The other is the Paleo-Kuril arc-trench system (made up by the Tokoro and Nemuro Belts) originated from subduction of Pacific plate under the Okhotsk plate under the southern or western margin of Okhotsk plate, it began it's activity in late Cretaceous (Kimura and Tamaki, 1985).

Tokoro Belt and Nemuro Belt in Shiranuka Hill area(Fig.1) are regarded as formed in the western or south-west margin of Okhotsk plate suggested by paleocurrent of the Nemuro Group in Shiranuka Hill and the occureance of high pressure type metamorphic rock in the Tokoro Belt

But the recent paleomagnetic study (Hamano et al.,1986) revealed that the fore-arc deposits of arc-trench system regarded as the part formed by eastward subducting were clockwise rotated.

For reconstructing the Cretaceous arc-trench system, the further paleomagnetic study was carried out on the Yusekyo Formation distributed on the westside of the Abashiri Tectonic Line in Hokkaido (Fig.1)

The Yusenkyo Formation consists of a large amount of terrigenous sediments (Kanamatsu et al.,1992). This formtion is characterized by the following features :1) The sediments of this formation are rich in intermediate volcanic materials (more than 90%). 2) Radiolarian fossils indicate late Cretaceous (late Campanian - early Maastrichtian) in age. These suggest that this formation accumlated in fore-arc basin of Paleo-Kuril arc.

PALEOMAGNETIC STUDY

In this study, the progressive A.F. demagnetization is effective to remove soft components for most pilot specimens. Figure 2 shows typical example of the ortogonal diagram of A.F. and thermal demagnetization. Most of specimens reveal 100 mA/m order in NRM intensity and have hight blocking temperature about 550-600°C. These characteristics probably arise from sedimentary compositions

DISCUSSION

Magnetic direction of Yusenkyo Formation revealing antipodal clusters. The mean direction (Dec. =136°,Inc. =43°) also reveal clockwise rotation as the Nemuro Group
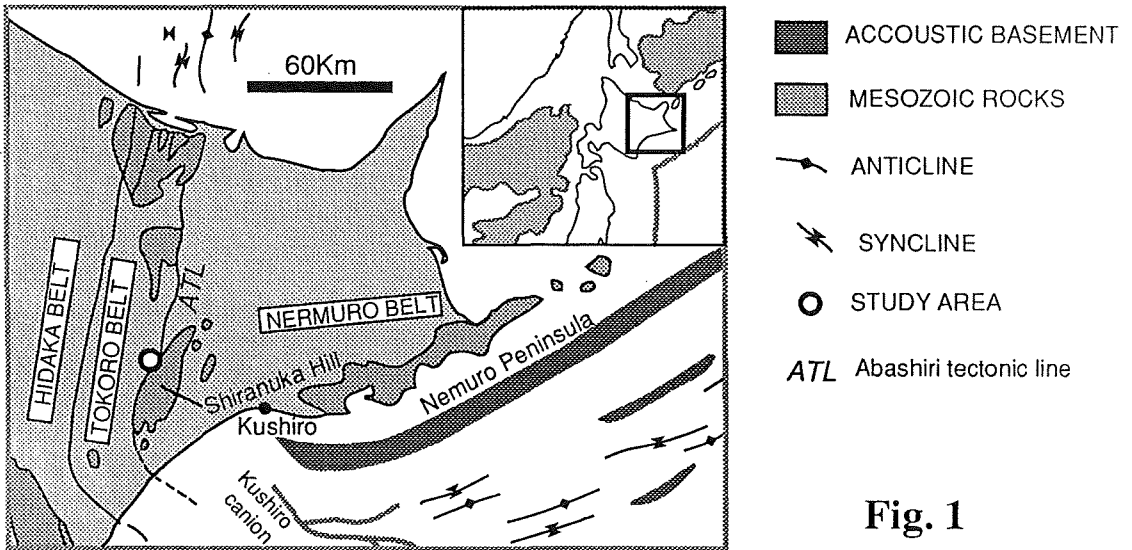
developing in Shiranuka Hill around K/T boundary (Dec. =73.2°,Inc. =39.5° ; Hamano et al, 1985), but more clockwise rotated.

From results of paleomagnetic studies, it is possible to say that the Nemuro Group in Shiranuka area and Yusenkyo Formation belonging to the TokoroBelt are reconstructed to be bent and placed in the western side of Nemuro Peninsula along the Kuril trench (Fig.3).

Since Miocene, the westward migration of fore-arc sliver of Kuril arc probably caused the deformation of the Shiranuka Hill area in westward convex form. After clockwise rotation, further rotations of Yusenkyo Formation might be possible in different sence, These differant clockwise directions may indicate the integrated amount of rotations since Cretaceous time.

REFERENCES
Hamano,Y.,Tsunakawa,H.,Saitou,Y. and Kikawa,E.(1986) Paleomagnetism of Hokkaido. Chikyu Monthly,8,434-439
Kanamatsu,T.,Nanayama,F.,Iwata,K. and Fujiwara,Y.(1992) Pre-Tertiary Systems on the western side of the Abashiri Tectonic Line in the Shiranuka area, eastern Hokkaido, north Japan: Implications to the tectonic relationship between the Nemuro and Tokoro Belts. Journal of Geological society of Japan,98
Kimura,G.(1986) Oblique subduction and collision. Geology,14,404-407
Kimura,G. and Tamaki,K.(1985) The Kuril Arc and Kuril Basin -The relationship between Rotation of Backarc Plate and Backarc Spreading.Journal of Geography,94,24-38
Niida,K. and Kito,N.(1986) Cretaceous arc-trench system in Hokkaido.Monograph of the Association for the. Geological Collaboration in Japan,31 379-402
Tanaka,H. and Uchimura,H.(1989) Tectonics of Hokkaido from the viewpoint of paleomagnetism, Chikyu monthly,11,298-306

Fig. 1

71233A;PAF
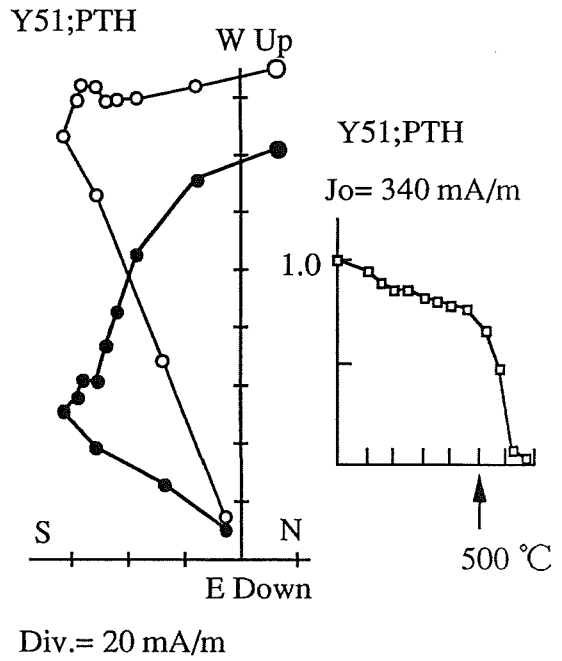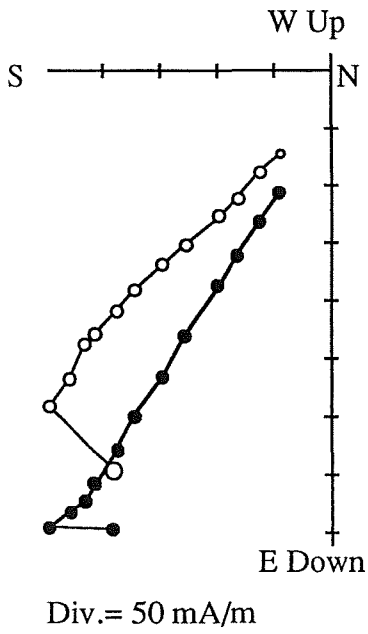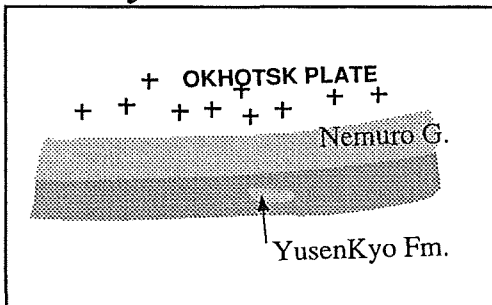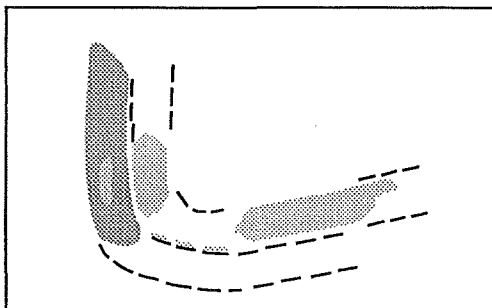

W Up

S ——————— N

E Down

Div.= 50 mA/m

Y51;PTH

W Up

S ——— N

E Down

Div.= 20 mA/m

Y51;PTH

Jo= 340 mA/m

1.0

500 ℃

Fig. 2

1 *early Cretaceous*

+ OKHOTSK PLATE
+ + + + + + + +

Nemuro G.

YusenKyo Fm.
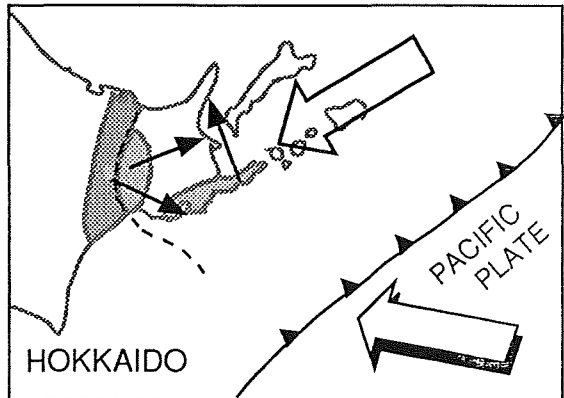
2 ?

3 *Miocene -*

PACIFIC PLATE

HOKKAIDO

Fig. 3

; Paleomagnetic declinations (Hamano et al.,1986,
Tanaka & Uchimura,1898 and This study)

PALEOMAGNETIC STUDY OF MIOCENE YOSHINO FORMATION, YAMAGATA PREFECTURE

Hiroyuki HOSHI[1], Masaki TAKAHASHI[2], and Kazuo SAITO[1]

1 Department of Earth Sciences, Faculty of Science, Yamagata
University, Yamagata 990, Japan
2 Geological Survey of Japan, Ibaraki 305, Japan

We made a paleomagnetic study on the Miocene Yoshino Formation in the Yamagata Prefecture to investigate the timing of an end of tectonic rotation of Northeast Japan(Fig.1). The Yoshino Formation distributed in the southernmost part of the Dewa Hill is composed mainly of submarine volcanic products, with intercalated argillaceous sediments. Hand samples of andesite(Kotaki Andesite) and rhyolite in this formation were selected for this study. The Kotaki Andesite is considered as submarine lava
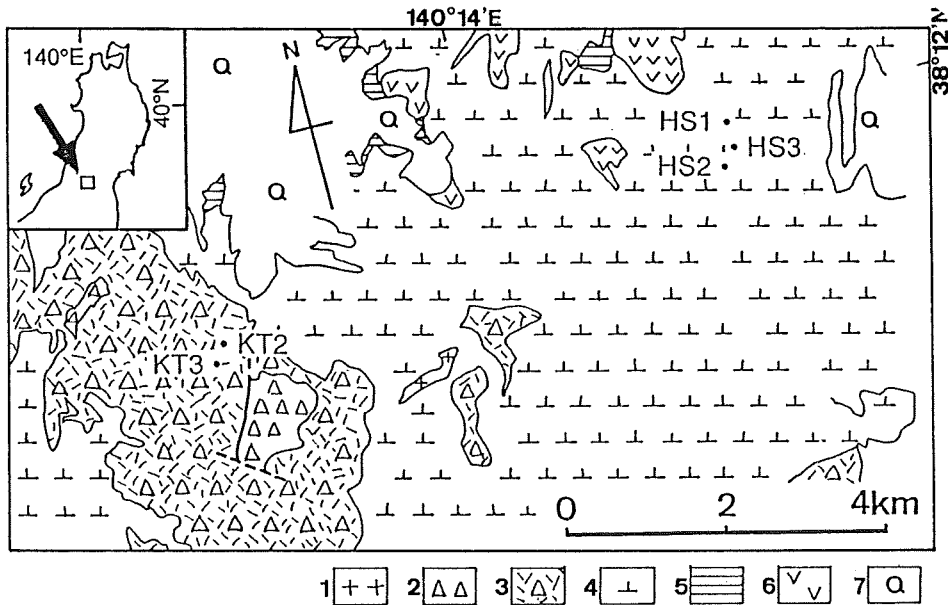

Fig.1. Geological map of the studied area(simplified from Kitamura,1986). 1=Granitic rocks; 2=Taro F.; 3=Lower Yoshino F.; 4=Upper Yoshino F.; 5=Hasedo F.; 6=Nomiokayama F.; 7=Quaternary volcanic rocks and pyroclastic flow deposits. Sampling sites are also marked on the map.

Stratigraphy			Lithology	Chronology
		Hasedo F.	Taffaceous sandstone , mudstone and acidic tuff	← CN5a *2
Yoshino F.	Upper	Ojirahu mudstone m.	Mudstone(intercalated with pumice tuff beds)	← CN5a *1
			Andesitic rocks , rhyolite , acidic pumice tuff and mudstone	*3 ←—15.3±0.5 (K-Ar) ← CN4 (early) *1
			Andesitic rocks(including Kotaki type andesite)	
	Lower	Simoyama mudstone m.	Mudstone	← CN4 *1
			Gravel-bearing andesitic lapilli tuff	
		Taro F.	Andesitic propylite , andesitic lapilli tuff	

Fig.2. Summary of stratigraphy and lithology of the southern part of the Dewa Hill.

*1: Okada(1979)
*2: Tamiya et al.(1986)
*3: Konda et al.(1986)

flows(hyaloclastites) and is overlying the Simoyama Mudstone Member conformably. The rhyolite which composes a main part of the lower division of the upper Yoshino Formation is also the hyaloclastites.

Nannofossils correlated to CN4 coccolith zone(Okada and Bukry, 1980) have been yielded from both the Simoyama Mudstone Member and the lower division of the upper Yoshino Formation(Okada, 1979;Fig.2). Nannofossils obtained from the Ojirahu Mudstone Member and the Hasedo Formation indicate the CN5a coccolith zone(Okada, 1979; Tamiya et al., 1986). Geochronometric age of the CN4/CN5 boundary is calibrated about 14.4Ma by Berggren et al.(1985). A K-Ar age of the rhyolite indicates 15.3±0.5Ma(Konda et al.,1986).

We collected 7 hand samples from 3 sites in a rhyolite body and 9 samples from 2 sites in the Kotaki Andesite. More than three cylindrical specimens were cored from each sample. After measurement of natural remanent magnetization(NRM), two pilot specimens were selected from each sample for demagnetization experiments. The results of the stepwise demagnetization are shown in Figure 3; here, ZH1 and ATH2 specimens are of the Kotaki Andesite, and DH1 and DH3 are of the rhyolite. The specimens of
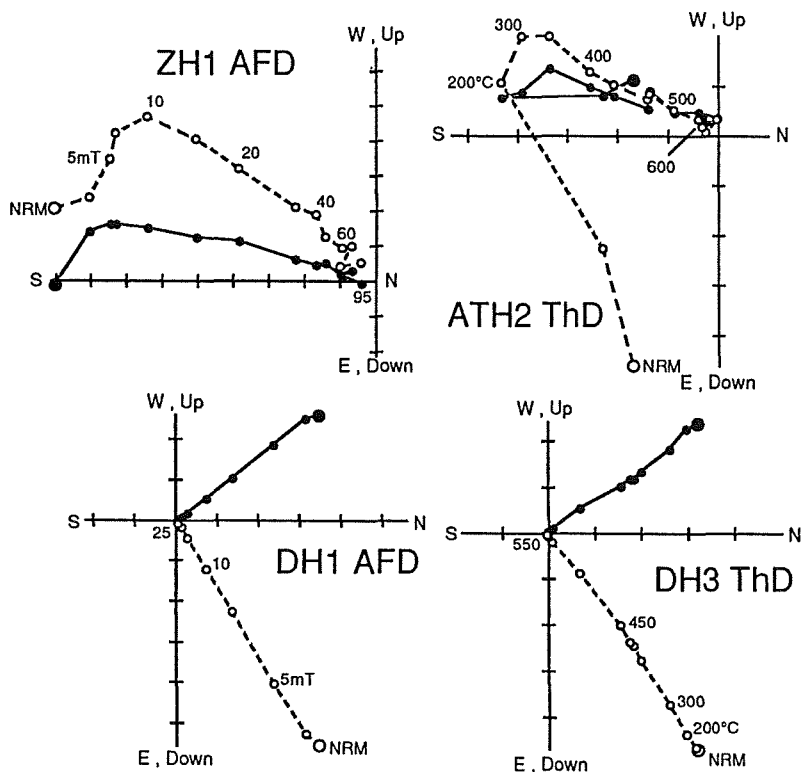
Fig.3. Behavior of vector endpoints of remanent magnetization. AFD and ThD denote alternating field demagnetization and thermal demagnetization, respectively. ZH1 and ATH2 are the pilot specimens from the Kotaki andesite, and DH1 and DH3 from a rhyokite body.

rhyolite show ideal behavior of the vector endpoints. On the other hand, the changes of remanent vectors of the specimens of the Kotaki andesite imply considerable overprinting of secondary magnetization. By the weak treatment of alternating field demagnetization(AFD) as well as thermal demagnetization(ThD), the secondary overprints could be removed. We conducted AFD for the whole specimens to erase the magnetic overprints.

The paleomagnetic results after appropriate demagnetization are listed in Table 1. Each site-mean direction of the rhyolite indicates a normal polarity and shows no deflected direction from the north. On the other hand, magnetization of the Kotaki Andesite is a reversed polarity. Figure 4 demonstrates an equal-area net projection of the each site-mean direction. These are *in-situ* directions. The geologic map and cross sections around the studied area(Adachi, 1977) show that the region has not been served any considerable deformation and regional tectonic disturbance. Inverting the
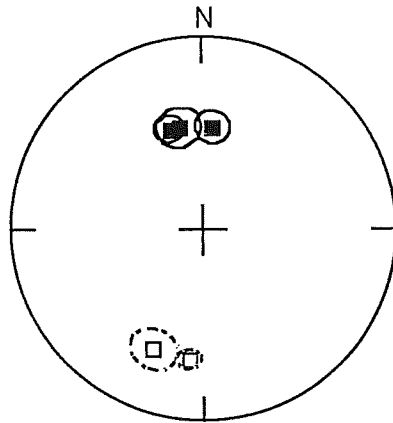
reversed polarity directions to the normal one, we obtained a formation mean direction of D=1.6°, I=40.5° and α_{95}=14.0°. The mean declination and inclination values almost correspond to the present geomagnetic field direction within the range of α_{95}. Paleomagnetic direction close to the recent geomagnetic field direction is often regarded to have the effects of secondary masking. However, as the both normal and reversed polarities are recognized and are making antipodal directions(Fig.4), the obtained direction may be the original one. The paleomagnetic character through the stepwise demagnetization also supports the reliability of the obtained data. Therefore, we can conclude that the southern part of the Dewa Hill is stationary since 15.3±0.5Ma. The rotation of Northeast Japan may have been terminated at about 15Ma.

Otofuji et al.(1985) proposed that Northeast Japan rotated counterclockwise between 21Ma and 14 to 11 Ma. Tosha and Hamano(1988) made a paleomagnetic study in the Oga Peninsula and concluded that Northeast Japan was rotated between 22 and 15. Recently, Yamazaki(1989) studied the Miocene strata in the Matsushima Bay area micropaleontologically and paleomagnetically, and concluded that the rotation of Northeast Japan was ceased at least 16Ma. Our results are concordant with a suggestion of Yamazaki(1989).

Table 1. Paleomagnetic results for the Yoshino Formation.

Site	N	n	Dec.	Inc.	$\alpha95$	k	VGP	Demag.
HS1	3	14	-13.5	44.3	9.1	20.2	73.0N , 91.3W	7.5mT
2	2	14	-18.7	43.6	6.0	44.9	70.3N , 93.7W	10mT
3	2	11	5.8	45.2	7.4	39.1	76.8N , 10.9W	15mT
KT2	4	16	-157.2	-31.9	9.5	16.2	62.0N , 10.5E	20mT
3	5	19	-173.1	-32.4	4.7	52.7	68.5N , 19.5W	15mT

N is the number of hand samples. n is the number of specimens. Dec.,Inc. and $\alpha95$ are declination , inclination and the radius of 95% confidence circle in degrees , respectively. k denotes the Fisher's precision parameter.VGP is latitude and longitude of the virtual geomagnetic pole position. Demag. is the level of alternating field demagnetization.

YOSHINO F.

Fig.4. Site mean directions and 95% confidence circles of the Yoshino Formation on an equal-area projection. Solid and open squares denote normal and reversed polarities, respectively.

References

Adachi,H.(1977)Jour.Geol.Soc.Jpn.,83,411.

Berggren,W.A.,D.V.Kent,J.J.Flynn, and J.A.Van Couvering(1985) Geol.Soc.Amer.Bull.,96,1407.

Kitamura,N.(ed.,1986)Cenozoic Tohoku-Honshu Arc geologic Data Series, vol.2(Hobundo,Sendai),8.

Konda,T.,K.Saito,Y.Watanabe, and H.Okada(1986)Jour.Geol.Soc.Jpn.,92,371.

Okada,H.(1979)Geol.Soc.Jpn.86th Annual Meeting Abstr.,104.

Okada,H. and D.Bukry(1980)Mar.Micropaleont.,5,321.

Otofuji,Y.,T.Matsuda, and S.Nohda(1985)Earth Planet.Sci.Lett.,75,265.

Tamiya,R.,T.Saito, and Y.Honda(1986)Geol.Soc.Jpn.93th Annual Meeting Field Trip Guide Book,143.

Tosha,T. and Y.Hamano(1988)Tectonics,7,653.

Yamazaki,T.(1989)Jour.Geomag.Geoelectr.,41,533.

PALEOMAGNETISM ON THE NORTHERN KYUSHU ISLAND: TECTONIC ON THE WESTERN PART OF THE CW-ROTATED SOUTHWEST JAPAN

Naoto ISHIKAWA

School of Earth Sciences, Faculty of Integrated Human Studies,
Kyoto University, Kyoto 606-01, Japan.

Introduction

Paleomagnetic investigations on and around the northern Kyushu Islands have documented the manner of the Middle Miocene clockwise (CW) rotation of Southwest Japan. Ishikawa et al. (1989) and Ishikawa and Tagami (1991) revealed the counter-clockwise (CCW) block rotations in the Tsushima Strait area at around 15 Ma, which constrained the western margin of the CW-rotated Southwest Japan block. The paleomagnetic direction of the Oligocene Ashiya Group indicated a CW rotation of the area including the Ashiya Group through about 28° (Ishikawa, 1990). Because pre-Neogene geologic units in the main part of the northern Kyushu Island (Main Kyushu) show approximate zonal arrangement, extending from the main part of Southwest Japan, the CW rotation was regarded as a rotational motion of Main Kyushu, namely the western part of Southwest Japan. The smaller rotation (~28°) was suggested for the western part of Southwest Japan when the main part was rotated through about 50°.

In order to clarify the manner of the CW rotation of Southwest Japan furthermore, paleomagnetic measurements were performed on samples from Tertiary sedimentary rocks at the following three areas in the northern Kyushu Island: the Sasebo-Imari, Amakusa, and Omuta areas (Fig. 1).
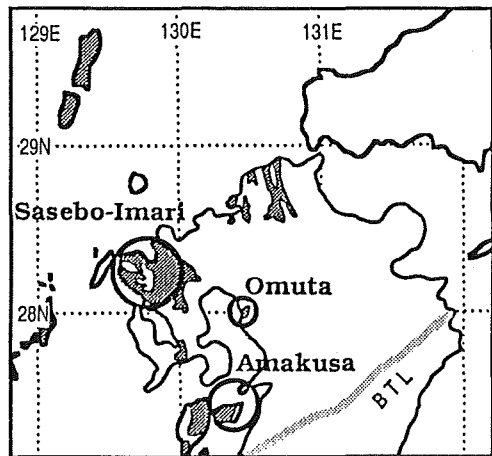

Fig. 1. Index map of studied areas. Shade areas indicate the distribution of Paleogene to Miocene sedimentary rocks in the northern Kyushu Island. BTL: Butsuzo Tectonic Line.

Sampling and paleomagnetic techniques

In the Sasebo-Imari area, tuff and mudstone samples were collected from the Kishima, Ainoura, and Sasebo Groups and the Oya Formation at 16 sites. Based on paleontological and radiometric age data (Kano et al., 1991; Okada, 1992), the geologic age of collected samples ranges from Oligocene to Early Miocene (about 30 Ma to 18 Ma). In the Amakusa area, paleomagnetic measurements were performed on samples from the Eocene Akasaki Group. Mudstone and sandstone samples with purple-red color were collected at eight sites in the Uto Peninsula and the Iwajima, Maejima and Kamishima islands. In the Omuta area, paleomagnetic samples were collected at eight sites of mudstone and sandstone with purple-red color from the Ginsui Formation, which has been correlated to the Akasaki Group in the Amakusa area.

Paleomagnetic samples were collected mainly using a gasoline-powered core drill and partially by hand sampling. Each site consists of six to fourteen core or block samples oriented by a magnetic compass. One or two standard cylindrical specimens or cubic specimens of about 20 mm were prepared from each sample.

The stability of natural remanent magnetization (NRM) was examined through progressive demagnetization experiments by thermal and alternating-field (AF) methods. NRM was measured by a cryogenic magnetometer (ScT C-112). Two or three pilot specimens from each site were subjected to progressive demagnetizations. When pilot demagnetization results yielded the stable components shown as straight line of vector-end points decaying toward the origin of Zijderveld diagram or the remagnetization circles on the equal-area projection, all remaining specimens of the site were progressively demagnetized. The direction of the stable component was obtained using principal component analysis (Kirschvink, 1980), anchored to the origin of the diagram. The common direction sheared by the remagnetization circles was calculated using the method of McFadden and McElhinny (1988), if available, combining the directions of the stable component. The site-mean direction with the radius of 95% confidence circle smaller than 20° was adopted as a characteristic direction of the site.

Characteristic directions

SASEBO-IMARI
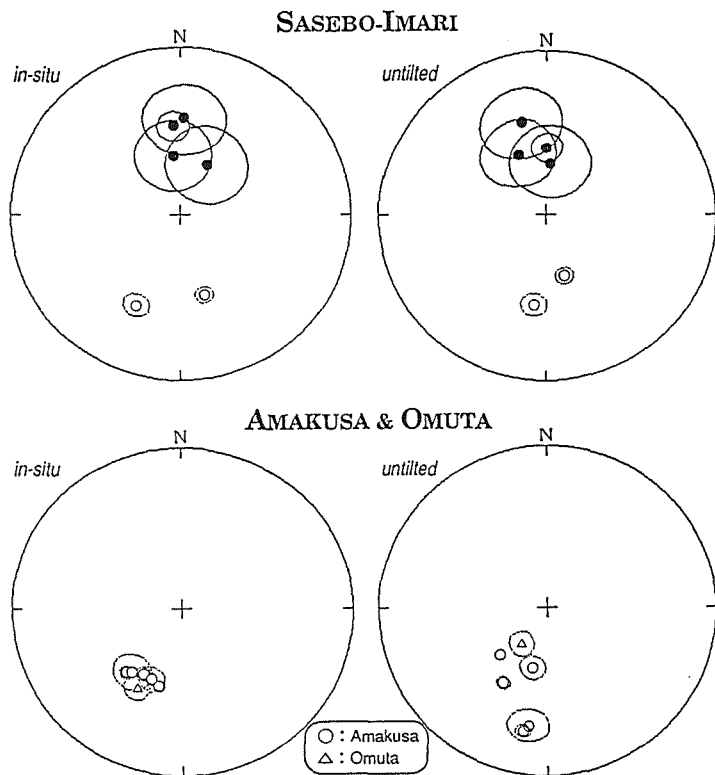

AMAKUSA & OMUTA

Fig. 2. Equal-area projections of in-situ and untilted site-mean directions from the Sasebo-Imari, Amakusa and Omuta areas. Solid and open symbols are on the lower and upper hemispheres, respectively. Ovals around the directions indicate 95% confidence limit.

Table 1. Paleomagnetic data from the Sasebo-Iamri, Amakusa and Omuta areas.

Site	N	levels	D	I	D*	I*	α_{95}	k
Sasebo-Imari area								
Oya Formation								
5	6	LA 360-620°C	-154.2°	-39.6°	-172.0°	-44.4°	6.0°	127.6
6	4	LA 320-560°C	2.5°	41.1°	-14.7°	39.6°	18.6°	25.4
Sasebo Group								
13	4	LA 10-25mT	-6.2°	59.8°	-23.5°	54.9°	18.1°	26.8
Ainoura Group								
12	6	LA 200-320°C	27.3°	61.5°	4.3°	62.0°	19.8°	12.4
Kishima Group								
10	6	LA 300-600°C	-4.5°	45.0°	0.6°	54.0°	7.5°	151.6
11	2	LA 5-20mT	163.4°	-48.6°	163.2°	-58.6°	4.3°	617.3
	2	GC 0-12.5mT						
MEAN	(6)			4.4°	50.4°		12.4°	30.3
MEAN*	(6)				-7.0°	52.9°	9.7°	48.8
	(	VGP	84.1° N	49.7° E	α_{95} = 11.1°	)		
Amakusa area (Akasaki Group)								
1	4	LA 590-680°C	-156.3°	-51.8°	-165.8°	-59.4°	6.1°	226.1
4	7	LA 360-650°C	-139.1°	-47.8°	-149.1°	-46.6°	3.2°	357.7
5	6	LA 360-650°C	-149.5°	-52.2°	-168.5°	-26.0°	3.4°	387.0
6	5	LA 560-650°C	-142.2°	-49.9°	-170.5°	-29.2°	9.0°	73.7
14	6	LA 590-680°C	-163.7°	-49.8°	-134.9°	-57.1°	2.3°	886.4
MEAN	(5)		-150.0°	-50.7°			6.4°	145.6
	(	VGP	64.7° N	145.2° W	α_{95} = 8.4°	)		
MEAN*	(5)				-159.1°	-44.4°	17.9°	19.1
Omuta area (Ginsui Formation)								
1	6	LA 580-660°C	-150.0°	-44.2°	-144.7°	-68.0°	6.0°	127.2

Note: Site: site number. N: number of specimens (sites). levels: demagnetization levels in which least-square line-fitting (LA) and least-square great circle fitting (GC) were applied after Kirschvink (1980) and McFadden and McElhinny (1988), respectively. D(D*),I(I*): declination and inclination in in-situ coordinates (after tilt correction), respectively. α_{95}: radius of 95% confidence circle. k:precision parameter. VGP:the north-seeking virtual geomagnetic pole position. The VGP for the Sasebo-Imari was calculated from the untilted site-mean directions, and that for the Amakusa area from the in-situ site-mean directions.

The characteristic directions were obtained from six sites in the Sasebo-Imari area (Table 1). The untilted directions showed a better antipodal relationship in a north-to-south trend than the in-situ directions (Fig. 2). The overall mean of the untilted directions was considered to be a mean paleomagnetic direction of the Kishima to the Nojima Groups, namely Oligocene to Early Miocene in the Sasebo-Imari area.

Five sites in the Amakusa area and one in the Omuta area yielded the stable components with higher unblocking temperature above 600°C during progressive thermal demagnetization (Table 1). The maximum AF demagnetization (100 mT) could not isolate the components similar to the higher temperature components. The demagnetization results indicated hematite to be the remanence carrier of the stable component. The site-mean directions of the components had southwest declination and negative inclination in in-situ coordinates (Fig. 2). The site-mean directions form the Amakusa area showed a tight cluster in in-situ coordinates, while the untilted directions were fairly scattered (Fig. 2). The common magnetic component of the Akasaki Group was regarded as a secondary component acquired after the formation of the fold system in the Amakusa area.

Discussion

The Virtual geomagnetic pole (VGP) for the secondary component directions from the Akasaki Group in the Amakusa area is different from the geographic pole, and it is close to the VGP for the Ashiya Group (Fig. 3). The discrepancy between the VGP for the Ashiya Group and the 30 Ma paleomagnetic pole for northern Eurasia (Irving and Irving, 1982) suggested the CW rotation of 28° for Main Kyushu (Ishikawa, 1990). The area from the Uto Peninsula to the Kamishima island is included in Main Kyushu from the view point of the zonal arrangement of pre-Neogene geologic units. The discrepancy between the VGP for the Akasaki
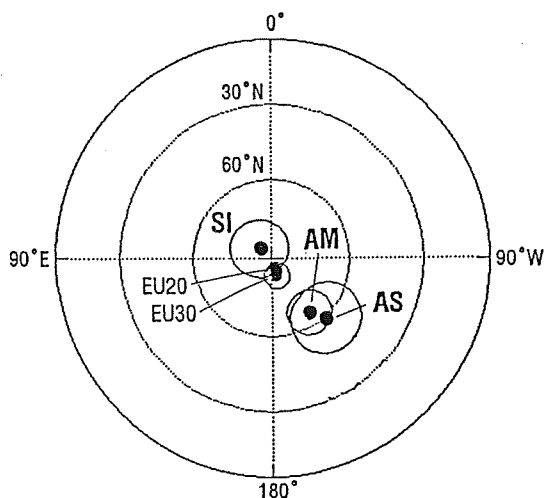
Fig. 3. Equal-area projections of virtual geomagnetic poles (VGP) for the Sasebo-Imari (SI) and Amakusa (AM) areas. EU20 and EU30 are northern Eurasia paleomagnetic poles for 20 and 30 Ma (Irving and Irving, 1982). AS is the VGP for the Ashiya Group [58.9° E and 137.9° W (α_{95} = 13.3°)] calculated from Ishikawa (1990).

Group and the geographic north can be explained by the CW rotation of Main Kyushu.

The VGP for the Sasebo-Imari area is close to the geographic north (Fig. 3). Taking the 20 Ma paleomagnetic pole of northern Eurasia as a reference, the paleomagnetic direction for the Sasebo-Imari area shows no significant discrepancies in both declination and inclination; the discrepancies in declination and inclination calculated based on the definitions of Beck (1980) and Demarest (1983) are $-12.6° \pm 12.9°$ and $1.7° \pm 8.0°$, respectively. It is indicated that the Sasebo-Imari area has been subjected to little significant tectonic displacement relative to northern Eurasia since about 30 Ma.

Because the zonal structure of the pre-Neogene geologic units in the main part of Southwest Japan is continuously traced to Main Kyushu (Ozawa, et al., 1984), the CW rotation of Main Kyushu can be attributed to the CW rotation of Southwest Japan (Ishikawa, 1990). In northwestern part of the Kyushu Island (NW Kyushu), the isolated pre-Neogene geologic units with N-S to NE-SW trending geologic structures, the high-P/T Nagasaki metamorphic rocks, are disposed. The significant difference in the structural trend of the pre-Neogene geologic units implies that NW Kyushu belongs to a different tectonic block from Southwest Japan (Kizaki, 1979, 1986; Faure et al., 1988). The paleomagnetic direction from the Sasebo-Imari area suggests that NW Kyushu did not suffer from the CW rotation of Southwest Japan. It is confirmed that the extent of Southwest Japan which experienced the Middle Miocene CW rotation is truncated at the west of Main Kyushu.

The CW rotation of Main Kyushu suggests a differential rotation between the main and the western part of Southwest Japan at the time of the CW rotation. Any large scale faults are not observed in geological features between the western and main part of Southwest. The ductile deformation might have been caused by the CW rotation of Southwest Japan around the boundary region. On the other hand, NW Kyushu seems to be separated by fault zone from Southwest Japan and the Tsushima Strait area. There is a large fault zone between the Tsushima Strait area and NW Kyushu, namely the Yobukonoseto Fault (Nagahama, 1962, 1965). The significant difference in the structural trend of pre-Neogene geologic units between NW Kyushu and Southwest Japan implies the existence of the fault zone in the boundary region (Hattori and Shibata, 1982). The Tertiary sediment sequences are distributed in the boundary region. Miki (1975) and Hattori and Shibata (1982) suggested that the sedimentary basins of the Tertiary sequences were formed as grabens.

The transpressional deformation event in the Tsushima Strait area occurred coeval with the CW rotation of Southwest Japan (Ishikawa and Tagami, 1991). The deformation event can be attributed to the CW rotation of Southwest Japan about a pivot placed on the western part (Ishikawa and Tagami, 1991). Associated with the convergence of the western margin of Southwest Japan at the CW rotation, NW Kyushu was probably translated northwestward. The paleomagnetic direction for the Sasebo-Imari area shows no significant tectonic displacement since about 30 Ma. However, the amount of the northwestward translation appears to be smaller than which can be detected significantly by means of paleomagnetism.

References

Beck, M. E., Jr. (1980) J. Geophys. Res., 85, 7115.

Demarest, H. H., Jr. (1983) J. Geophys. Res., 88, 4321.

Faure, M., O. Fabbri, and P. Monie (1988) Earth Planet. Sci. Lett., 91, 105.

Hattori, H. and K. Shibata (1982) Bull. Geol. Surv. Japan, 33, 57.

Irving, E. and G. A. Irving (1982) Geophys. Surveys, 5, 141.

Ishikawa N. (1990) Rock Mag. Paleogeophys., 17, 73.

Ishikawa N. and T. Tagami (1991) J. Geomag. Geoelectr., 43, 229.

Ishikawa, N., M. Torii, and K. Koga (1989) J. Geomag. Geoelectr., 41, 797.

Kano, K., H. Kato, Y. Yanagisawa and F. Yoshida (1991) Report Geol. Surv. Japan, 274, pp. 114.

Kirschvink, J. L. (1980) Geophys. J. R. astr. Soc., 62, 699.

Kizaki, K. (1979) Earth Sci., 33, 144.

Kizaki, K. (1986) Tectonophysics, 125, 193.

McFadden, P. L. and M. W. McElhinny (1988) Earth Planet. Sci. Lett., 87, 161.

Miki, T. (1975) Mem. Fac. Sci., Kyushu Univ., Ser. D, Geol., 23, 165.

Nagahama, H. (1962) Jour. Geol. Soc. Japan, 68, 199.

Nagahama, H. (1965) Report, Geol. Surv. Japan, 211, pp. 72.

Okada, H. (1992) Jour. Geol. Soc. Japan, 98, 509.

Ozawa, T., A. Taira, and F. Kobayashi (1985) Kagaku (Science), 55, 4.

(To be submitted to J. Geomag. Geoelectr.)

CLOCKWISE ROTATION OF THE RED RIVER FAULT INFERRED FROM PALEOMAGNETIC STUDY OF CRETACEOUS ROCKS IN THE SHAN-THAI- MALAY BLOCK OF WESTERN YUNNAN, CHINA

Shoubu FUNAHARA*†, Nobukazu NISHIWAKI*, Fumiyuki MURATA**,
Yo-ichiro OTOFUJI* and Yi Zhao WANG***

* Department of Earth Sciences, Faculty of Science, Kobe University, Kobe 657, Japan
** Department of Management and Information, Osaka Junior College, Osaka 587, Japan
*** Yunnan Bureau of Geology and Mineral Resources, Kunmin, China

More than 150 samples were collected at 23 sites from the Lower Cretaceous Jingxing Formation around the city of Yongping (25.5°N, 99.5°E) (see Fig. 1) which is located on the west side of the Red River fault. Sixteen sites have characteristic directions with high temperature component above 500°C. The high temperature component magnetization from 12 sites is pre-fold origin, and reveals clockwise deflection in declination (Dec=42.0°, Inc=51.1°, and α_{95}=15.7°). The easterly declination more than 40 ° of Yongping is consistent with the Cretaceous paleomagnetic direction (Dec=45°) of Chuxiong (25°N, 101.5°E) which is located on the east side of the Red River fault (Funahara et al., 1992). Both areas were subjected to about 25° clockwise rotation with respect to the eastern part of the Yangtze block since the Cretaceous time. We conclude that the Red River fault was rotated through 25°± 16° with respect to the eastern part of the Yangtze block associated with rotation of the Yongping and Chuxiong areas. Removal of the rotation from the Red River fault indicates that the Red River fault and the Jinsha suture formed a straight line along N55°W-S55°E within the Asian continent from Vietnam to the Tibetan Plateau in the present coordinate system at the Cretaceous time (Fig. 1). The lectilinear feature of the Red-River fault and Jinsha suture was deformed to the present unusually curved shape probably due to collision of the Indian continent to the Asian continent.

REFERENCES

Besse, J. and V. Courtillot, Revised and synthetic apparent polar wander paths of the African, Eurasian, North American and Indian Plates, and true polar wander since 200 Ma, J. Geophys. Res., 96, 4029, 1991.

† On January 3, 1991, he disappeared in an avalanche at the Mt. Meylixueshan (6740m) in the Yunnan Province of China. He has been missing since then.
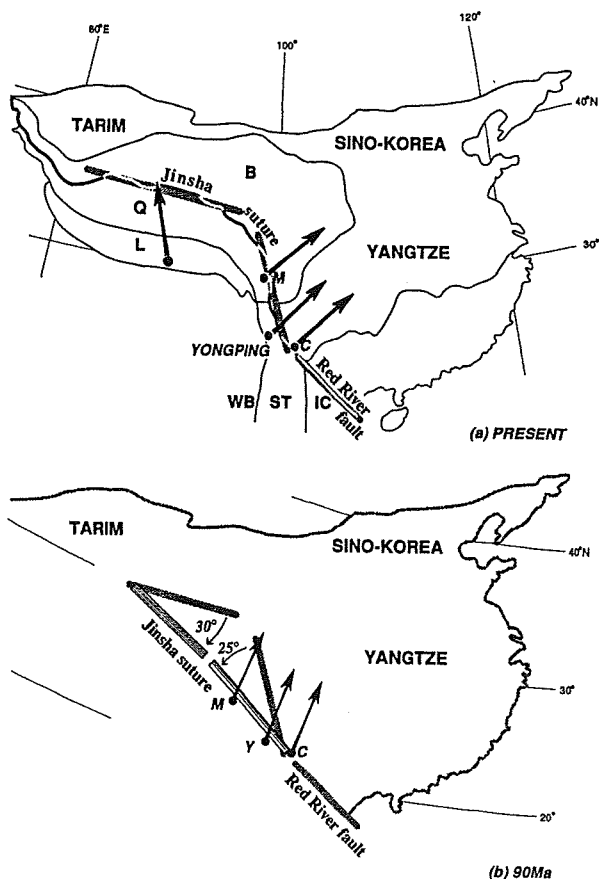
Fig. 1.   Arrangement in the Red River fault-Jinsha suture at the present and at 90 Ma in the Cretaceous time.
       (A) Present: The Red River fault-Jinsha suture is curvelineal in shape. This curvelineal shape is divided into three portions. The northern portion with strike of N80°W in the Tibetan Plateau, the central portion with the strike of N15°W in the Three Rivers region and the southern portion along the Red River with a strike of N55°W. The solid arrow marks the observed declination of the Cretaceous rocks at the Yongping (Y), Chuxiong (C), Markam (M) and Lhasa (L). L=Lhasa Terrane, Q=Qiangtang Terrane, B=Bayan Kala Terrane, WB=West Burman block, ST=Shan-Thai-Malay block, IC=Indochina block.
       (B) 90 Ma: Ancestral feature of the Red River fault-Jinsha suture is reconstructed. Chuxiong and the southern portion of the Red River fault-Jinsha suture are arranged in their present relative positions with whole China block. The northern portion is restored by clockwise rotation through 30°, and the central portion is rotated counter-clockwise through 25°. Ancestral strikes of the northern and central portions are N60°W and N40°W in the present coordinate system at the Cretaceous time, respectively. The ancestral feature is expected to be rectilineal in the Cretaceous time. The Cretaceous paleomagnetic directions at Yongping, Chuxiong, and Markam become nearly parallel to the Cretaceous paleomeridian associated with the reconstruction of the Red river and the Jinsha suture. The paleolatitude in the Cretaceous is calculated from the pole at 90 Ma (77°N, 200°E) (Besse and Courtillot, 1991).

(submitted to Earth Planet. Sci. Lett.)

HIGH RESISTANCE OF CONTINENTAL LITHOSPHERE OF TARIM CRATON ALONG THE ALTYN TAGH FAULT AGAINST ITS LARGE SLIP MOVEMENTS -- K-Ar DATING AND PALEOMAGNETIC STUDY--

Yo-ichiro OTOFUJI[1], Tetsumaru ITAYA[2], Shaoshun WANG[3]
and Susumu NOHDA[4]

1) Department of Earth Sciences, Faculty of Science, Kobe University, Kobe 657, Japan
2) Hiruzen Research Institute Okayama Branch, Okayama University of Science, Okayama 700, Japan
3) Institute of Geology, Academia Sinica, Beijin, China
4) Kyoto Sangyo University, Kamigamo, Kita-ku, Kyoto 603, Japan

Two basaltic andesite lavas from the Puru area (36°15′N; 81°30′E) along the Altyn Tagh fault (see Fig. 1) are dated by K-Ar methods: their ages are 1.05 ± 0.11 Ma and 1.44 ± 0.06 Ma, respectively. Both lower and upper lava flows are well grouped and all of reversed magnetic polarity. Paleomagnetic direction of 3 sites of the lower lava flow is D=172.0°, I=-55.6°, α_{95} =3.0°, whereas that of 10 sites of the upper one is D=-167.0°, I=-51.0°, α_{95} =2.1°. The mean paleomagnetic direction of the two lava flows is D=-176.9°, I= -53.8°.
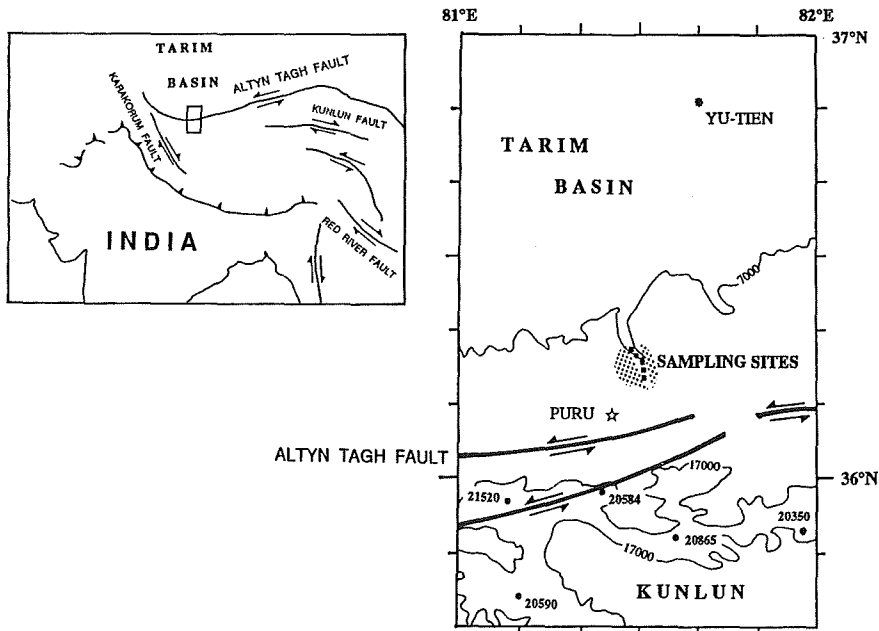

Fig. 1.   Location map showing some features of geography and geology around the Puru area. Sampling areas are shown by a chain of the squares. Heavy lines are the Altyn Tagh fault after Peltzer et al. (1989). Dotted patterns show the area of out crop of Quaternary basaltic andesite lava flows. Number of the elevation contour and summits are shown in feet after the map of ONC G7 (1987).

Paleomagnetic study and K-Ar dating indicate that the Puru area has undergone little rotation (less than 3.1° in clockwise sense) during the last 1.4 m.y. Although the studied area is located at 13 km north of the Altyn Tagh fault, the area has never experienced rotational motion during the large slip of the fault more than 42 km in the last 1.4 m.y. (Peltzer et al.,1989). We conclude that little deformation penetrates into the Puru area. High resistance to the deformation of the continental lithosphere along the Altyn Tagh fault is explained by a rigid material of the continental lithosphere along the fault and/or a smooth slip of the Altyn Tagh fault. Since the Altyn Tagh fault is probably a simple strike-slip fault associated with little convergence or divergence, the stress acting on the Altyn Tagh fault is not strong enough to deform or destroy the continental lithosphere along it.

REFERENCES

Operational Navigation Charts G7, scale 1:1,000,000, Defence Mapping Agency, ed. 7, St. Louis, 1987.

Peltzer, G., P. Tapponnier and R. Armijo, Magnitude of Late Quaternary left-lateral displacements along the north edge of Tibet, Science, 246, 1285, 1989.

(submittedt to Earth Planet. Sci. Lett.)

MAGNETIZATION OF SEAMOUNTS INFERRED FROM DOWNHOLE THREE COMPONENTS MAGNETOMETER LOGS

Yoshifumi NOGI[1] , Hisao ITO [2] and ODP Legs 143 and 144 Scientific Parties

1Geochemical Laboratory   2 Geothermal Research Department
Meteorological Research Institute   Geological Survey of Japan
1-1 Nagamine,Tsukuba 305   1-1-3 Higashi, Tsukuba 305

1 Introduction

The ODP Legs 143 and 144 constitute of drilling Cretaceous reef-bearing guyots of the Western Pacific (Fig. 1), with the objectives of using them as monitors of relative sea-level changes and thereby of the combined effects of the tectonic subsidence (and uplift) history of the seamounts and of global fluctuations of sea level. We have investigated the magnetization of seamounts with downhole three components magnetometers. Japanese downhole magnetometer was used for Leg 143 and the Schlumberger GPIT data were analyzed for the Leg 144. Drilling on Leg 143 occurred at four sites: the summits of two guyots in the Mid Pacific Mountains (Sites 865, 866 and 867/868); and archpelagic adjacent to paired atoll guyot in the Marshall Islands (Site 869), and within the lagoon of a modern Marshall Islands atoll (Site 870) . The Japanese magnetometer measured three components of the geomagnetic field within Holes 865A, 866A and 869A. Leg 144 constitutes of twenty drillings at ten sites (Limalok Guyot; Site 871, Lo-En Guyot; Site 872, Wodejebato Guyot; Sites 873 through 877, MIT Guyot Site 878 and Seiko Guyot; Sites 879 and 880) and logging at Hole 801C drilled in old Jurassic oceanic crust during Leg 129. GPIT data were obtained for Sites 873A, 874A, 801C, 878A and 879A. We present the results of downhole magnetometer measurements obtained in basaltic layers of seamounts (865A, 866A, 873A, 878A and 879A) .

2 Downhole Magnetometer
### 1) Japanese magnetometer

The Japanese downhole three components magnetometer was designed and fabricated for downhole measurements in ODP and DSDP holes. The magnetometer is composed of four high-pressure vessel sections, which are made of MONEL alloy.

The downhole magnetometer measures temperature and the three orthogonal components of the magnetic field. Ring-core fluxgate-type magnetic sensors are used for detecting the magnetic field. Three mutually perpendicular ring cores, drive coils, and pick-up coils are installed in the bottom section of the magnetometer. The fluxgate sensor is drived by 15 kHz and the detection circuit converts the amplitude of higher harmonics, which is proportional to the external field strength in the sensor detection, to the DC output voltage. The signal from three magnetic sensors and temperature sensor were digitized by a sixteen bits A/D converter and then stored in IC memory in the downhole instrument. The downhole magnetometer is operated by the internal batteries with the maximum operating time of twelve hours. The data were transferred to the personal computer after the downhole measurements were finished.

The maximum resolution of the downhole magnetometer is 1.02 nT and was calibrated by a Helmholtz coil at the Kakioka Magnetic Observatory. Sampling interval is 3 seconds.

2) Schlumberger GPIT (General Purpose Inclinometer Tool)

A three axis flux gate magnetometer is attached to the Formation MicroScanner tool. Data on the orientation and strength of the magnetic field within the borehole is collected at 15cm (0.50 ft) intervals, while the Formation MicroScanner image data has a 2.5 mm sampling rate. The three components magnetic data enable calculation of horizontal intensity, inclination and relative declination. The magnetic direction is used to orient the Formation MicroScanner traces with respect to magnetic north.
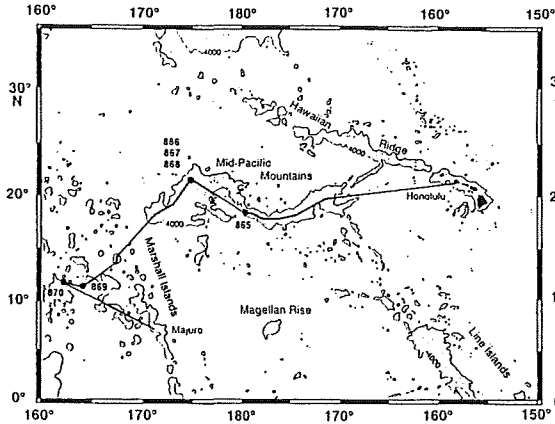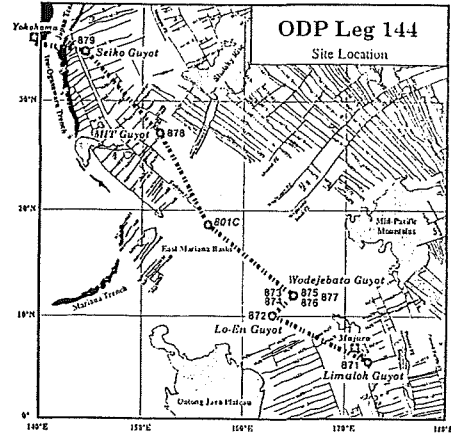
Fig. 1 (a) The location of Leg 143 drill sites and the track of the drill ship. Sea floor shallower than four km is striped.
(b) The location of Leg 144 drill sites and the track of the drill ship (after Nakanishi et al.,1992).

3 Results and Discussions

1) Hole 865A

Hole 865A was drilled between the summit of the pelagic cap and the south rim of Allison Guyot in the western Mid Pacific Mountains. The hole penetrated 870.9 mbsf (meters below sea floor), through 140m of pelagic cap, and 698m of shallow water limestone before bottoming in 33m of basaltic sills intruded limestone. The Japanese magnetometer measured three components of the geomagnetic field within Hole 865A from 500 to 865 mbsf. From the observed three components of the magnetic field, the horizontal and the vertical component of the magnetic field inside the hole were calculated. Fig.2 shows both the horizontal and vertical magnetic field. There are sharp decreases in the horizontal magnetic field with very high amplitude above 650 mbsf. These variations were caused by abrupt changes in the tool orientation. However the variations of horizontal and vertical magnetic field at 650 to 830 mbsf are rather smooth. Their vales are almost the same as the IGRF87 field (IAGA Division I Working Group 1, 1987). This indicates that surrounding materials above 830 mbsf (mainly limestone) are little magnetized. Below 830 mbsf, there are three obvious peaks in both the horizontal and vertical magnetic field component; at about 840, 845 and 857 mbsf. At about 853 mbsf, there is also an obvious peak in the horizontal component, while it is obscure in the vertical component. These four peaks almost coincide with the basaltic layers. The character of these peaks shows that the magnetization of basaltic layer has a negative inclination and normal directions of declination which were acquired in the southern hemisphere during the normal polarity chron.

2) Hole 866A

Hole 866A (Heuvo Guyot) was located in the Mid Pacific Mountains 716 km to the northwest of Hole 865A. The hole penetrated 1743.6 mbsf, coring approximately 1620m of shallow water limestone overlying about 124m of basalt. The magnetometer measured three components of the geomagnetic field from 1595 to 1636 mbsf (Fig.3). The horizontal

and the vertical components of the geomagnetic field are shown in Fig.3. At about 1622 mbsf, the vertical component of the geomagnetic field decreases abruptly. The horizontal component of the geomagnetic field also decreases at the same sub bottom depth. These decrease coincide with the shallowest basaltic layer within the hole and are caused by the strong magnetization of basaltic layer.

Decrease in the vertical magnetic field below 1622 mbsf indicates that the magnetization of basaltic layer has a positive inclination. Between 1622 and 1630 mbsf, the horizontal component of magnetic field also decreases. However, a sharp jump in the horizontal component occurs at about 1630 mbsf and the horizontal magnetic field increases below 1630 mbsf. This indicates that the declination of the basaltic layer between 1622 and 1630 mbsf has the reverse direction and turns to the normal direction below 1630 mbsf. The basaltic layer section 1622 mbsf is divided into two layers by the declination of the magnetization. Normal declination below 1630 mbsf may be caused by the secondary magnetization of highly altered basalt and/or volcanic breccias.

3) Hole 873A

Hole 873A was drilled to 232 mbsf on Wodejebato Guyot. Two passes of the Formation MicroScanner measurements extended down to 225 mbsf and the upper limit of the Formation MicroScanner measurements was the base of the drill string at 51 mbsf, located within the pelagic sediments overlying the carbonate platform (Fig. 4). Within the carbonate section, the magnetometer appears to be recording only the ambient present day field. These limestones are little magnetized.

At about 175 mbsf coinciding with the clay/basalt boundary, there are sharp decrease in both the vertical and horizontal component of the downhole magnetic field. These show that magnetization of the basaltic layers were obtained in the southern hemisphere during the reverse polarity chron. This is consistent with the shipboard paleomagnetic results for recovered core samples. The fine scale variations in the observed magnetic field with depth were duplicated on the two Formation MicroScanner passes, indicating that these variations probably correlate with distinct basaltic or weathering horizons.
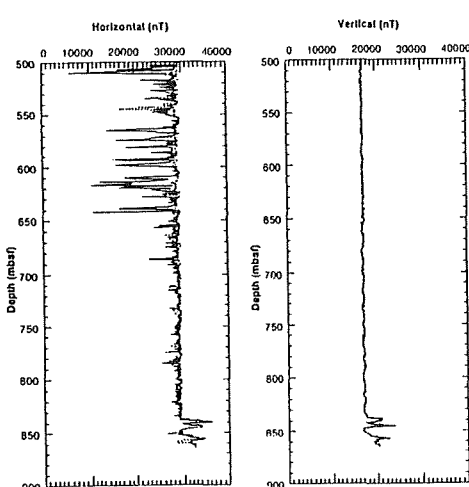

Fig.2 Variations of horizontal and vertical components of the geomagnetic field,obtained by theJapanese downhole magnetometer within Hole 865A. Solid and broken lines show going down and up log, respectively.
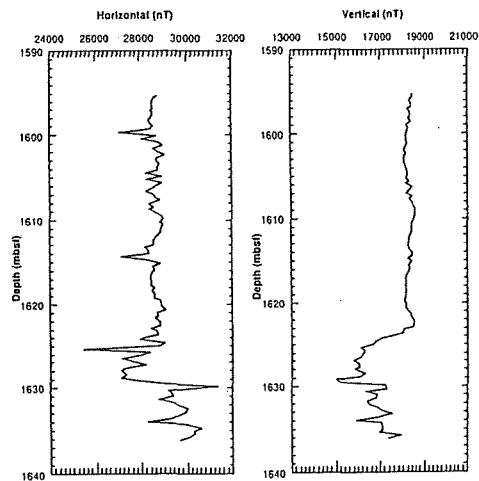
Fig.3 Variation of the horizontal and vertical component of the geomagnetic field obtained by the Japanese down-hole magnetometer within Hole 866A.

4) Hole 878A

Two stages of the measurements were made for the FMS tool. The first stage of the measurements (two passes; Run 1 and Run 2) were made for the lower igneous complex from 807 mbsf to 885 mbsf corresponding to Cores 144-878A-87R through -94R, with the drill pipes above 2144.3 m below rig floor (806.7 mbsf). Then the carbonate platform series was logged (two passes; Run 3 and Run 4) from 10 mbsf to 735 mbsf.

The total magnetic field data for the upper carbonate platform series is almost in agreement with the ambient present day geomagnetic field, while both the vertical and horizontal intensities have slight offsets from the ambient present day geomagnetic field. In addition, the horizontal intensities have several jumps. These offsets in the vertical and horizontal intensities are duplicated during the Run 3 and Run 4, while the jumps in the horizontal intensity are not.

The vertical, horizontal and total magnetic intensities for the basaltic basement (810 mbsf to 880 mbsf) are generally smaller than the ambient present day geomagnetic field intensities. These features suggest that the magnetization of the basalt below about 850 mbsf was acquired in the southern hemisphere during the reverse polarity chron. However, the magnetization of basalt above this depth was not known because there were no measurements due to the unstable hole condition.

5) Hole 879A

Two passes of the measurements were made for the FMS tool from about 216 mbsf to 36 mbsf for the complete carbonate platform and igneous complex in Hole 879A in the southern rim of Seiko Guyot (Fig. 6).

There is a sharp increases in both the vertical and horizontal intensities of the downhole magnetic field at 190 mbsf. These correspond to boundaries for breccia/weathered basalt. These might be interpreted as the magnetization of the weathered basalt was obtained in the southern hemisphere during the normal polarity chron.
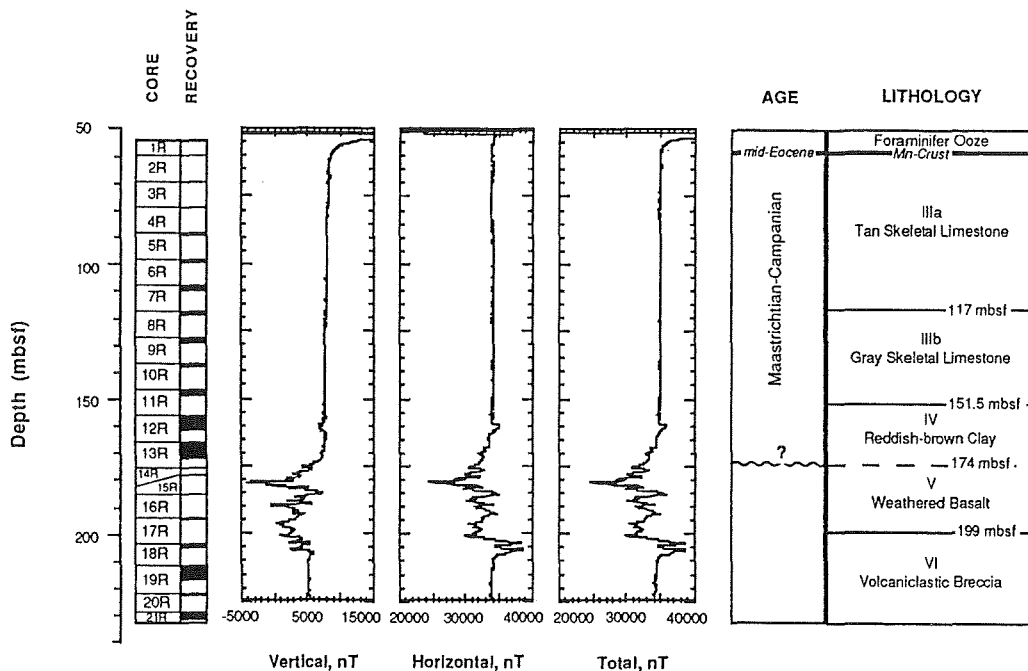

Fig.4 Variation of the magnetic field obtained by Schlumberger GPIT and core data for Hole 873A.
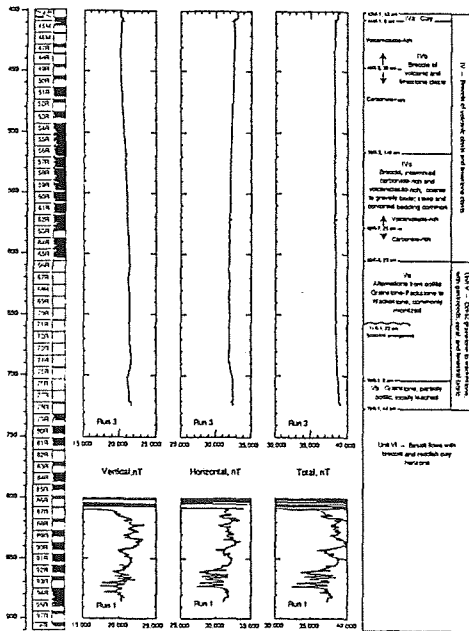
Fig. 5 Variation of the magnetic field
obtained by Schlumberger GPIT and
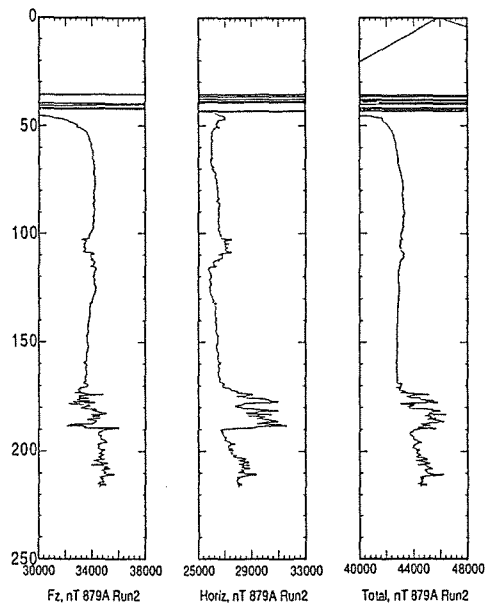core data for Hole 878A.

Fig. 6 Variation of the magnetic field
obtained by Schlumberger GPIT for
Hole 879A.

References

IAGA Division I Working Group 1, J. Geomagn. Geoelectr., 37:1175-1164,1987.
Nakanishi, M. K.Tamaki, K.Kobayashi, Geophys. Res. Lett., 693-696.
Nakanishi, M. K.Tamaki, K.Kobayashi, Geophys.J.Int., 109,701-719, 1992.

SIMILAR CHARACTERISTIC OF MAGNETIC DIRECTION CHANGE

- IN THE CASE OF JAPAN SEA AND SOUTH CHINA SEA

Yukari NAKASA

Earthquake Research Institute, University of Tokyo, Bunkyo-ku, Tokyo 113

There are many marginal basins located in the Northwestern Pacific region (Fig. 1). Japan Sea and South China Sea might have some similarities from the viewpoint of not only general topographic shape but also the seismic and magnetic data (Tamaki, 1991). Both marginal basins have oceanic and continental crust, and on the oceanic crust, some magnetic linealities could be identified. Making histograms of the magnetic anomalies which reveal lineated magnetic patterns in the Japan Basin, Japan Sea. Seama and Isezaki (1990) identified the presence of a weakly lineated anomaly pattern trending N60°E-N40°E. Three lineation trends; N30°-35°E, N65°E, and N70°-75°E, for the eastern, central and western Japan Basin, respectively, are identified. Neither symmetrical anomaly patterns or spreading axes were recognized.

Research on the Japan Sea magnetics has been ongoing since the first studies of Yasui (1967). Isezaki and Uyeda (1973) suggested the presence of a magnetic anomaly lineation pattern in the Japan Sea with a strike of N60°E. Isezaki (1973, 1975) further mapped probable magnetic lineations. However, because of generally low and a contour map of magnetic anomalies (< 300 nT) and an apparent discontinuous lineation pattern, these studies did not identify specific reversals or ascribe ages to the pattern. Isezaki (1986) made a magnetic anomaly contour map of the entire Japan Sea. Seama and Isezaki (1990) mapped magnetic lineations trending N40°E and N60°E divided by a magnetic boundary area in the northeast part of the Japan Basin.

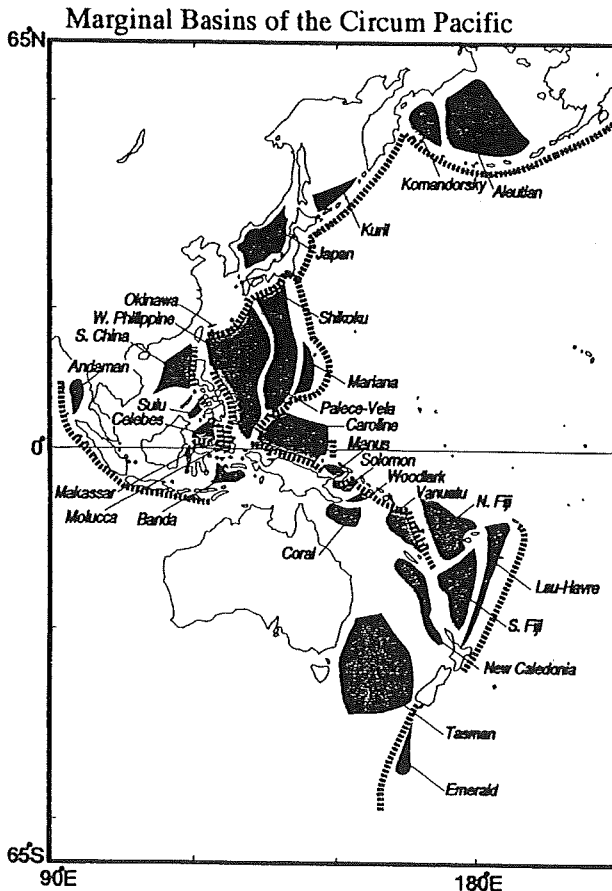## Marginal Basins of the Circum Pacific

Figure 1 Marginal basins around the Pacific Ocean compiled by Tamaki and Honza (1991). Solid areas show marginal basins, and blocked lines show trenches.

Marine geomagnetic data for this study include all available Japan Sea data from the National Geophysical Data Center (NGDC) of the National Oceanic and Atmospheric Administration (NOAA), U.S.A., and from the Japan Oceanographic Data Center (JODC). Table 1 lists these data, including data obtained from many scientific cruises up to 1986 by the Geological Survey of Japan (GSJ), Japan Maritime Safety Agency (JMSA), Ocean Research Institute (ORI), Japan Meteorological Agency (JMA) and institutions of the U.S.A. and Russia. To work with the magnetic anomalies are systematically shifted from zero level to correct the biasing of IGRF (International Geomagnetic Reference Field) (Isezaki, 1973a; Matsumoto and Isezaki, 1989). All refined data calculated on the basis of IGRF90 were used. Satellite positioning data made by the Navy Navigation Satellite System (NNSS), Global Positioning System (GPS), Long Range Navigation System (LORAN-C) and hybrid system were selected.

In an area of the Japan Basin within a rectangle of 39°N-43°N, 131°E-138°E, the presence of some magnetic anomaly lineation has been pointed out by Isezaki and Uyeda (1973), Isezaki (1973, 1975), Seama and Isezaki (1990). Firstly, making grid data of magnetic anomalies using Akima's method (1970, 1974) and Fig. 3 is a magnetic anomaly contour map by Briggs' method (1974). Then re-confirmation of the direction of magnetic anomaly lineations. Calculating average amplitude of magnetic anomaly each 1° interval same direction on longitudinal lines (Fig. 4); 132°E, 133.5°E, 135°E, 137°E, and divided four small rectangles; (40°-43°N, 132°-133.5°E), (40°-43°N, 133.5°-135°E), (40°-43°N, 135°-137°E), (40°-43°N, 137°-138°E). Each longitudinal line shows boundary of directions of lineation pattern. Plotting data on histograms in order to clarify lineation contrasts. Arrows show prominent anomaly contrasts.

There are also magnetic linearities with several directions on the South China Sea Basin. Taylor and Hayes (1983) suggested that evolution of the South China Sea changed from north-south spreading in the eastern basin. Pigott and Ru (1988) suggested two stage of spreading and three rifting episodes from changing trend of magnetic lineations. Briais et al. (1989) used Seabeam data to present that there may be an alternative explanation to the east-west and northwest-southeast trending magnetic anomalies. Lee and Lawver (1992) mentioned the whole opening history of the South China Sea examining structural fabrics, paleostress patterns, available geological data, and paleomagnetic data as well as the

Table 1-1

No	Cruise-ID	Survey Year	Country/Institution
1	SF6702	1972	Japan/Kobe Univ. Seifu-maru
2	SF669999	1966	Japan/Kobe Univ. Seifu-maru
3	SF6701	1967	Japan/Kobe Univ. Seifu-maru
4	SF6605	1966	Japan/Kobe Univ. Seifu-maru
5	SF6604	1966	Japan/Kobe Univ. Seifu-maru
6	SF6603B	1966	Japan/Kobe Univ. Seifu-maru
7	SF6603A	1966	Japan/Kobe Univ. Seifu-maru
8	SF6602	1966	Japan/Kobe Univ. Seifu-maru
9	SF6601	1966	Japan/Kobe Univ. Seifu-maru
10	SF659999	1965	Japan/Kobe Univ. Seifu-maru
11	SF650699	1965	Japan/Kobe Univ. Seifu-maru
12	SF650599	1965	Japan/Kobe Univ. Seifu-maru
13	SF6504	1965	Japan/Kobe Univ. Seifu-maru
14	SF6503A	1965	Japan/Kobe Univ. Seifu-maru
15	SF6502	1965	Japan/Kobe Univ. Seifu-maru
16	SF6501	1965	Japan/Kobe Univ. Seifu-maru
17	SF6401	1964	Japan/Kobe Univ. Seifu-maru
18	YUK1B	1970	Japan/Kobe Univ. Daici-maru
19	YUK1A	1970	Japan/Kobe Univ. Daici-maru
20	LUM1	1970	Japan/Kobe Univ. Daici-maru
21	KUM1	1970	Japan/Kobe Univ. Daici-maru
22	OM1	1970	Japan/Kobe Univ. Daici-maru
23	KOFU	1970	Japan/Kobe Univ. Kofu-maru
24	HS8304	1983	Japan/Hydro.Dep. Shoyo
25	HS7505	1975	Japan/Hydro.Dep. Shoyo
26	HS7201	1972	Japan/Hydro.Dep. Shoyo
27	HM7602	1976	Japan/Hydro.Dep. Meiyo
28	HM7503	1975	Japan/Hydro.Dep. Meiyo
29	HM7401	1974	Japan/Hydro.Dep. Meiyo
30	HM7302	1973	Japan/Hydro.Dep. Meiyo
31	HM7202	1972	Japan/Hydro.Dep. Meiyo
32	HM7201	1972	Japan/Hydro.Dep. Meiyo
33	HM7103	1971	Japan/Hydro.Dep. Meiyo
34	HM7004	1970	Japan/Hydro.Dep. Meiyo
35	HM7002	1970	Japan/Hydro.Dep. Meiyo
36	HM6903	1969	Japan/Hydro.Dep. Meiyo
37	HM6902	1969	Japan/Hydro.Dep. Meiyo
38	HM6804	1968	Japan/Hydro.Dep. Meiyo
39	HM6703	1967	Japan/Hydro.Dep. Meiyo
40	HT6501	1965	Japan/Hydro.Dep. Meiyo
41	GH7802	1978	Japan/GSJ
42	GH7703	1977	Japan/GSJ
43	GH7702	1977	Japan/GSJ
44	GH7602	1976	Japan/GSJ

Table 1-1 (continued)

No	Cruise-ID	Survey Year	Country/Institution
45	KH7004	1970	Japan/ORI/UT
46	KH6902	1969	Japan/ORI/UT
47	KH6701	1967	Japan/ORI/UT
48	DME21	1978	USSR/Dm.Mendeleev
49	DME10	1973	USSR/Dm.Mendeleev
50	DME07	1971	USSR/Dm.Mendeleev
51	DM7-A	1971	USSR/Dm.Mendeleev
52	DM6	1971	USSR/Dm.Mendeleev
53	DME06	1971	USSR/Dm.Mendeleev
54	DME05-B	1971	USSR/Dm.Mendeleev
55	DM5-B	1971	USSR/Dm.Mendeleev
56	VIT53	1972	USSR/VITYAZ
57	VI51	1972	USSR/VITYAZ
58	VI49	1970	USSR/VITYAZ
59	VI47	1970	USSR/VITYAZ
60	ST	1969	USSR/VITYAZ
61	VI42	1967	USSR/VITYAZ
62	VIT51	1972	USSR/VITYAZ
63	SI343912	1979	USA/USNS/NAVOCEANO
64	SI343619	1976	USA/USNS/NAVOCEANO
65	SI343608	1975	USA/USNS/NAVOCEANO
66	SI938029	1968	USA/USNS/NAVOCEANO
67	SI938023	1968	USA/USNS/NAVOCEANO
68	V3311	1976	USA/LAMONT-DOHERTY/VEMA
69	V3312	1976	USA/LAMONT-DOHERTY/VEMA
70	V3213	1975	USA/LAMONT-DOHERTY/VEMA
71	V3212	1975	USA/LAMONT-DOHERTY/VEMA
72	V2815	1971	USA/LAMONT-DOHERTY/VEMA
73	C1218	1969	USA/LAMONT-DOHERTY/VEMA
74	DSDP31GC	1973	USA/SCRIPPS INST./GLOM.CHAL.
75	ZTES2BAR	1966	USA/SCRIPPS INST./ARGO.
76	ZTES04AR	1966	USA/SCRIPPS INST./ARGO.
77	ZTES03AR	1966	USA/SCRIPPS INST./ARGO.

Table 1   List of cruise data used in this study. Data come from the National Geophysical Data Center (NGDC), 1986-version.

regional tectonic history of the surrounding area of the South China Sea Basin. ·

The similar characteristic of changing magnetic trend both in the Japan Sea and the South China Sea may suggest that many faults have been affecting. In order to reveal tectonic history of such a complicated continental margin area, more systematic and concentrated survey will be required. Japan and China joint study on the tectonic evolution of the South China Sea is just running from the fiscal year of 1991. Actual onboard research will be started performing explosive refraction survey at the northern margin to the oceanic basin area as the first phase of the project on the middle of May, 1993. Major objective of the first phase study is to determine the boundary between deep and intermediate seismic structure and magnetic quiet zone along north-south direction line with 350 *km* length including eight points heat flow measurement survey. The further project will be developed after qualification and assessment of the results of the first phase research. It might be great helpful to understand more detail historical and predictable formation process of some marginal basins.
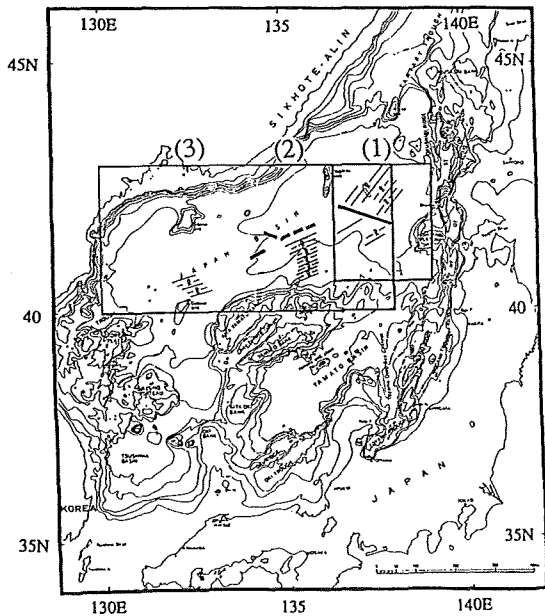
Figure 2 Re-examination area of magnetic anomaly of the Japan Sea (hatched area). Solid lines are magnetic lineation patterns, N and R are Normal and Reverse magnetization, respectively. Small rectangular areas indicate research area in this study, number(1) area by Seama and Isezaki (1990) and Tamaki and Kobayashi (1988), thick solid line is interpreted as a boundary where the trend of the magnetic lineations changes (Seama and Isezaki 1990). Number (2) and (3) show different direction of anomaly pattern.

Figure 3 Contour map of magnetic anomaly of the Japan Basin (40°N-43°N, 130°E-138°E).
Table 1 shows data source of this map. Contour interval is 20 nT and dark area show positive anomalies and light area show negative.
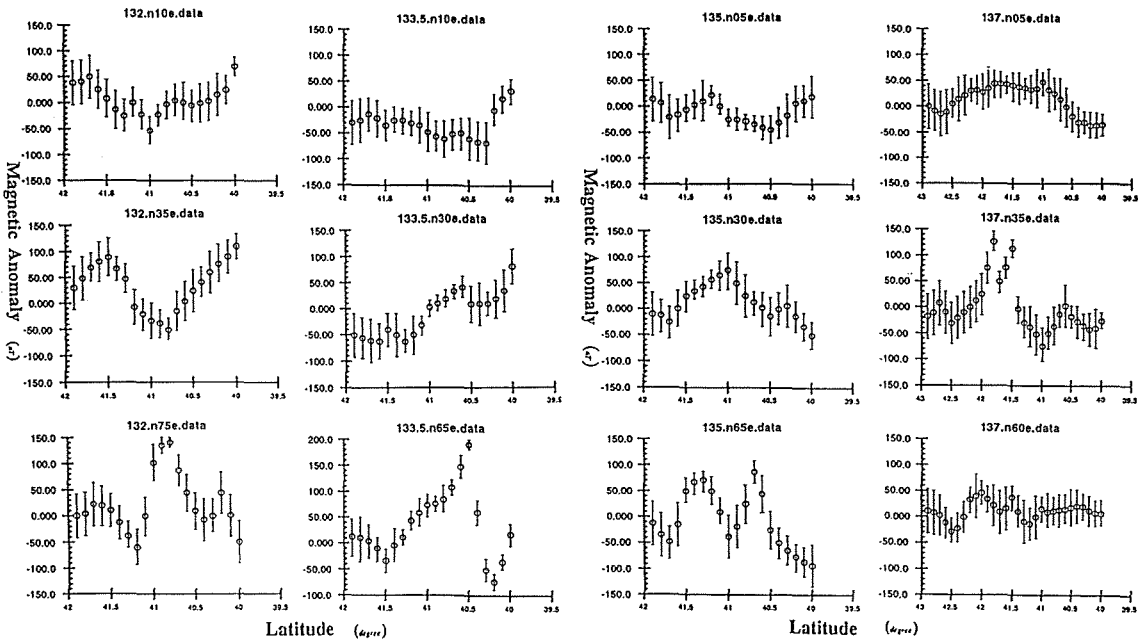
Magnetic Anomaly
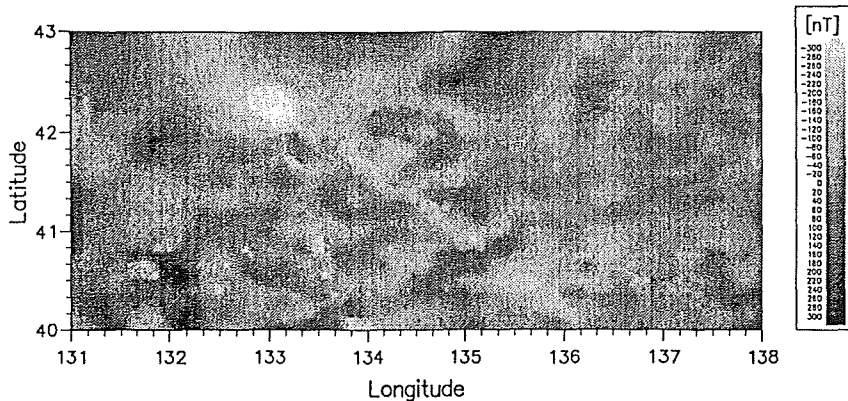
Figure 4 Calculating average amplitude of magnetic anomaly from 132°E to 138°E, devided four parts with standard deviation ±1σ . Arrows show four prominent magnetic anomaly contrasts.

References

Akima, H. (1970) J. Acm., 17, 589.

Briais, A., P. Tapponnier, and G. Pautot (1989) Earth Planet. Sci. Lett., 95, 307.

Briggs, I. G. (1974) J.G.R., 39, 39.

Isezaki, N. (1973) Oceanogr. Magazine, 24, 107.

Isezaki, N. and S. Uyeda (1973) Marine Geophys. Res., 2, 51.

Isezaki, N. (1975) Marine Geophys. Res., 2, 265.

Isezaki, N. (1986) J. G. G., 38, 403.

Isezaki, N. and Y. V. Shevaldin (1991) Japan-USSR Monograph Series 1.

Kobayashi, K. and N. Isezaki (1976) Geophys. Monogr. Ser. 19, 235.

Kobayashi, K., K. Tamaki, M. Nakanishi, N. Isezaki, and K. Sayanagi (1986) EOS, 67, 44, 1227.

Kobayashi, K. (1988) Preliminary Report of the Hakuho Maru Cruise KH86-2, Ocean Res. Inst., Univ. Tokyo, 129.

Lee, T. Y. and Lawver, L. A. (1992) J. Geol. Soc. China, 35, 353.

Matsumoto, K. and N. Isezaki (1989) B.C.thesis (in Japanese), Kobe University.

Pautot, G., C. Rangin, et al. (1986) Nature, 321, 150.

Ru, K. and D. Pigott (1986) Bull. Amer. Asso. Petrol. Geol., 70, 1136.

Seama, N. and N. Isezaki (1990) Tectonophy., 181, 285.

Tamaki, K. (1986) J. G. G., 38, 427.

Tamaki, K. and K. Kobayashi (1988) Mar. Sci. Mon. (in Japanese), 20, 705.

Tamaki, K., K. Kobayashi, N. Isezaki, K. Sayanagi, M. Nakanishi, and C. H. Park, (1988) preliminary Report of the Hakuho Maru Cruise KH86-2, 7.

Tamaki, K. and E. Honza (1991) Episodes, 14, 224.

Tamaki, K. and K. Pisciott, et al. (1992) Proc. ODP, Init. Repts. 127, College Station, 1478.

Taylor, B. and D. E. Hayes (1983) Geophys. Monogr. Ser., 27, 23.

Yasui, M., Y. Hashimoto, and S. Uyeda (1967) Oceanogr. Magazine, 19, 221.

SOME NOTES ON CALCULATING VGP

Hidetoshi SHIBUYA

Dep't Earth Sci., C.I.A.S., Univ. Osaka Pref., Sakai 593, JAPAN

The way how to calculate the position of VGP (virtual geomagnetic pole) in virtually all the text books (from McElhinny, 1973, to Butler, 1992) is as follows:
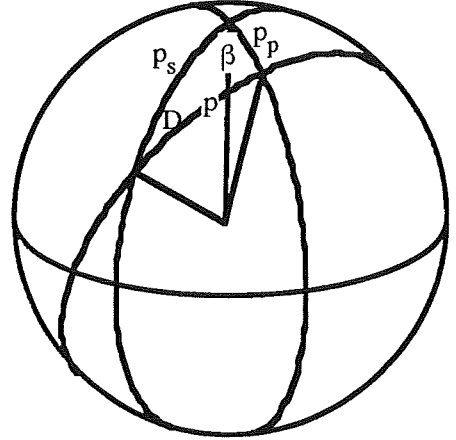
$$p = \tan^{-1}\left(\frac{2}{\tan I}\right) \qquad (1)$$

$$\lambda_p = \sin^{-1}(\sin\lambda_s \cos p + \cos\lambda_s \sin p \cos D) \qquad (2)$$

$$\beta = \sin^{-1}\left(\frac{\sin p \sin D}{\cos\lambda_p}\right) \qquad (3)$$

$$\phi_p = \phi_s + \beta \qquad \text{if } \cos p \geq \sin\lambda_p \sin\lambda_s \qquad (4a)$$
$$\phi_p = \phi_s + \pi - \beta \qquad \text{if } \cos p < \sin\lambda_p \sin\lambda_s \qquad (4b)$$

where λ_p and λ_s are VGP and site latitude, ϕ_p and ϕ_s are VGP and site longitude, D and I are Declination and Inclination of paleomagnetic direction, respectively. Equation 3 is derived from the sine theorem

$$\frac{\sin\beta}{\sin p} = \frac{\sin D}{\sin p_p} \qquad (5)$$

and Equation 4 is from cosine theorem

$$\cos p = \cos p_p \cos p_s - \sin p_p \sin p_s \cos\beta \qquad (6)$$

on sphere, where p_p and p_s are VGP and site colatitude, respectively. In this scheme, the longitude of VGP is calculated with the sine theorem and the range of the arcsine is determined with the cosine theorem.

These theorems can be used in the other way. The longitude of VGP may be calculated with the cosine theorem and the range of the arccosine is, then, determined with the sine theorem. The formulation is,

$$\beta = \cos^{-1}\left(\frac{\cos p_p \cos p_s - \cos p}{\sin p_p \sin p_s}\right) \qquad (7)$$

$$\phi_p = \phi_s + \beta \qquad \text{if } \frac{\sin D \sin p}{\sin p_p} \geq 0 \qquad (8a)$$

62

$$\phi_p = \phi_s - \beta \qquad \text{if} \quad \frac{\sin D \sin p}{\sin p_p} < 0 \qquad (8b)$$

The advantage of the later scheme is that the sign of the second part of equation (8) depends only on the sign of $\sin D$, because sine of colatitude is always positive in all over the domain. Taking the domain of declination, D, from $-\pi$ to π, the sign of $\sin D$ is the same as the sign of D. Thus, the ϕ_p is easily given as

$$\phi_p = \phi_s + \cos^{-1}\left(\frac{\cos p_p \cos p_s - \cos p}{\sin p_p \sin p_s}\right)\text{sign}(D) \qquad (9)$$

where $\text{sign}(D)=1$ if $D>=0$ and $\text{sign}(D)=-1$ if $D<0$. Note that some computer programming languages give $\text{sign}(0)=0$. Careless programming may give wrong results at $\beta=\pi$. Practically, it is written as:

$$\phi_p = \phi_s + \cos^{-1}\left(\frac{\sin \lambda_p \sin \lambda_s - \cos p}{\cos \lambda_p \cos \lambda_s}\right)\text{sign}(D) \qquad (10)$$

This scheme may not give any improvement in accuracy nor calculating speed, but it makes the programming much easier and avoids possible programming errors.

References
McElhinny (1973) Palaeomagnetism and plate tectonics (Camgridge University Press, Camgridge), p.25.
Butler (1992) Paleomagnetism (Blackwell Scientific Publications, Boston), pp.158-159.

Authors Index